1 Results and Discussion

1.1 Results: ΛK^0_S and $\Lambda K^{\pm}$

In the following sections, we present results assuming (i) three residual contributors (Sec. 1.1.1), (ii) ten residual contributors (Sec. 1.1.2), and (iii) no residual correlations (Sec. 1.1.3). Comparisons of results obtained using different variations of the fit method, including different numbers of residual contributors, can be found in Sec. 1.1.4.

For the results shown, unless otherwise noted, the following hold true: All correlation functions were normalized in the range $0.32 < k^* < 0.40$ GeV/c, and fit in the range $0.0 < k^* < 0.30$ GeV/c. For the ΛK^- and $\bar{\Lambda}K^+$ analyses, the region $0.19 < k^* < 0.23$ GeV/c was excluded from the fit to exclude the bump caused by the Ω^- resonance. The non-femtoscopic backgrounds for the ΛK^+ and ΛK^- systems were modeled by a (6^{th}-)order polynomial fit to THERMINATOR simulation, while those for the ΛK^0_S were fit with a simple linear form. All analyses were fit simultaneously across all centralities, with a single radius and normalization λ parameter for each centrality bin. Scattering parameters ($\Re f_0$, $\Im f_0$, d_0) were shared between pair-conjugate systems, but assumed unique between the different ΛK charge combinations (i.e. a parameter set describing the ΛK^+ & $\bar{\Lambda}K^-$ system, a second set describing the ΛK^- & $\bar{\Lambda}K^+$ system, and a third for the ΛK^0_S & $\bar{\Lambda}K^0_S$ system). Each correlation function received a unique normalization parameter. The fits were corrected for finite momentum resolution effects, non-femtoscopic backgrounds, and residual correlations resulting from the feed-down from resonances.

Lines and boxes on the experimental data represent statistical and systematic errors, respectively. In the figures showing experimental correlation functions with fits, the black solid curve represents the primary (ΛK) correlation's contribution to the fit. The green line shows the fit to the non-flat background. The purple points show the fit after all residual contributions have been included, and momentum resolution and non-flat background corrections have been applied. The extracted fit values with uncertainties are printed as (fit value) $\pm$ (statistical uncertainty) $\pm$ (systematic uncertainty).

1.1.1 3 Residual Correlations Included in Fit

Figure 2 nicely collects and summarizes all of our extracted fit parameters for the case of 3 included residual contributors. In the summary plot, we show the extracted scattering parameters in the form of a $\Im f_0$ vs $\Re f_0$ plot, which includes the d_0 values to the right side. We also show the λ vs. radius parameters for all three of our studied centrality bins. The extracted fit parameters are also collected in Table **??**. Figure 3 presents our extracted fit radii, along with those of other systems previously analyzed by ALICE [**?**], as a function of pair transverse mass (m_{T}).

Figure 2 nicely collects and summarizes all of our extracted fit parameters for the case of 3 included residual contributors. Figure 3 presents our extracted fit radii, along with those of other systems previously analyzed by ALICE [**?**], as a function of pair transverse mass (m_{T}). Figures 4, 5, and 6 show the experimental correlation functions with fits, assuming 3 residual contributors, for all studied centralities for ΛK^0_S with $\bar{\Lambda}K^0_S$, ΛK^+ with $\bar{\Lambda}K^-$, and ΛK^- with $\bar{\Lambda}K^+$, respectively. The parameter sets extracted from the fits can be found in Tables 5 and 6.

Figures 5, 6, and 4 show the experimental correlation functions with fits, assuming 3 residual contributors, for all ΛK systems (ΛK^+, ΛK^-, and ΛK^0_S, respectively) in all studied centralities. The parameter sets extracted from the fits can be found in Table **??**. Figures with a wider range in k^*, showing better the non-femtoscopic background, may be found in Appendix **??**. Also contained in Appendix **??** are plots demonstrating the contributions from the residuals, as well as results assuming 10 and no residual contributors.

In Figures 5 - 4, the pair system (e.g. ΛK^+) data is shown in the left column, and the conjugate pair system (e.g. $\bar{\Lambda}K^-$) in the right The rows differentiate the different centrality bins (0-10% in the top,

Centrality	λ	R
0-10%	1.40 $\pm$ 0.63 (stat.) $\pm$ 0.17 (sys.)	6.24 $\pm$ 0.92 (stat.) $\pm$ 0.66 (sys.)
10-30%	0.90 $\pm$ 0.34 (stat.) $\pm$ 0.17 (sys.)	4.41 $\pm$ 0.50 (stat.) $\pm$ 0.39 (sys.)
30-50%	1.00 $\pm$ 0.34 (stat.) $\pm$ 0.22 (sys.)	3.51 $\pm$ 0.44 (stat.) $\pm$ 0.28 (sys.)

System	$\Re f_0$	$\Im f_0$	d_0
ΛK^+ & $\bar{\Lambda} K^-$	-0.49 $\pm$ 0.19 (stat.) $\pm$ 0.12 (sys.)	0.42 $\pm$ 0.22 (stat.) $\pm$ 0.12 (sys.)	-0.55 $\pm$ 2.22 (stat.) $\pm$ 1.76 (sys.)
ΛK^- & $\bar{\Lambda} K^+$	0.19 $\pm$ 0.15 (stat.) $\pm$ 0.08 (sys.)	0.29 $\pm$ 0.17 (stat.) $\pm$ 0.08 (sys.)	-7.80 $\pm$ 6.15 (stat.) $\pm$ 6.10 (sys.)
ΛK^0_S & $\bar{\Lambda} K^0_S$	0.09 $\pm$ 0.15 (stat.) $\pm$ 0.06 (sys.)	0.53 $\pm$ 0.28 (stat.) $\pm$ 0.13 (sys.)	-2.59 $\pm$ 1.47 (stat.) $\pm$ 3.59 (sys.)

Table 1: Fit Results ΛK, with 3 residual correlations included. The fit procedure is as described in the text. The fit is done on the data with only statistical error bars. The errors marked as "stat." are those returned by MINUIT. The errors marked as "sys." are those which result from my systematic analysis (as outlined in Section **??**).

10-30% in the middle, and 30-50% in the bottom). The lines on the data represent the statistical errors, while the boxes represent the systematic errors. The fit procedure is as described in the text; in short, all systems are fit simultaneously with shared radii, while each [ΛK^+, ΛK^-, ΛK^0_S] maintains a unique set of scattering parameters. The black solid line represents the primary ΛK component of the fit. The green line shows the fit to the non-flat background. The purple points show the fit after all residuals' contributions have been included, and momentum resolution and non-flat background corrections have been applied. The extracted fit values with uncertainties are printed in the top left panel of each figure.

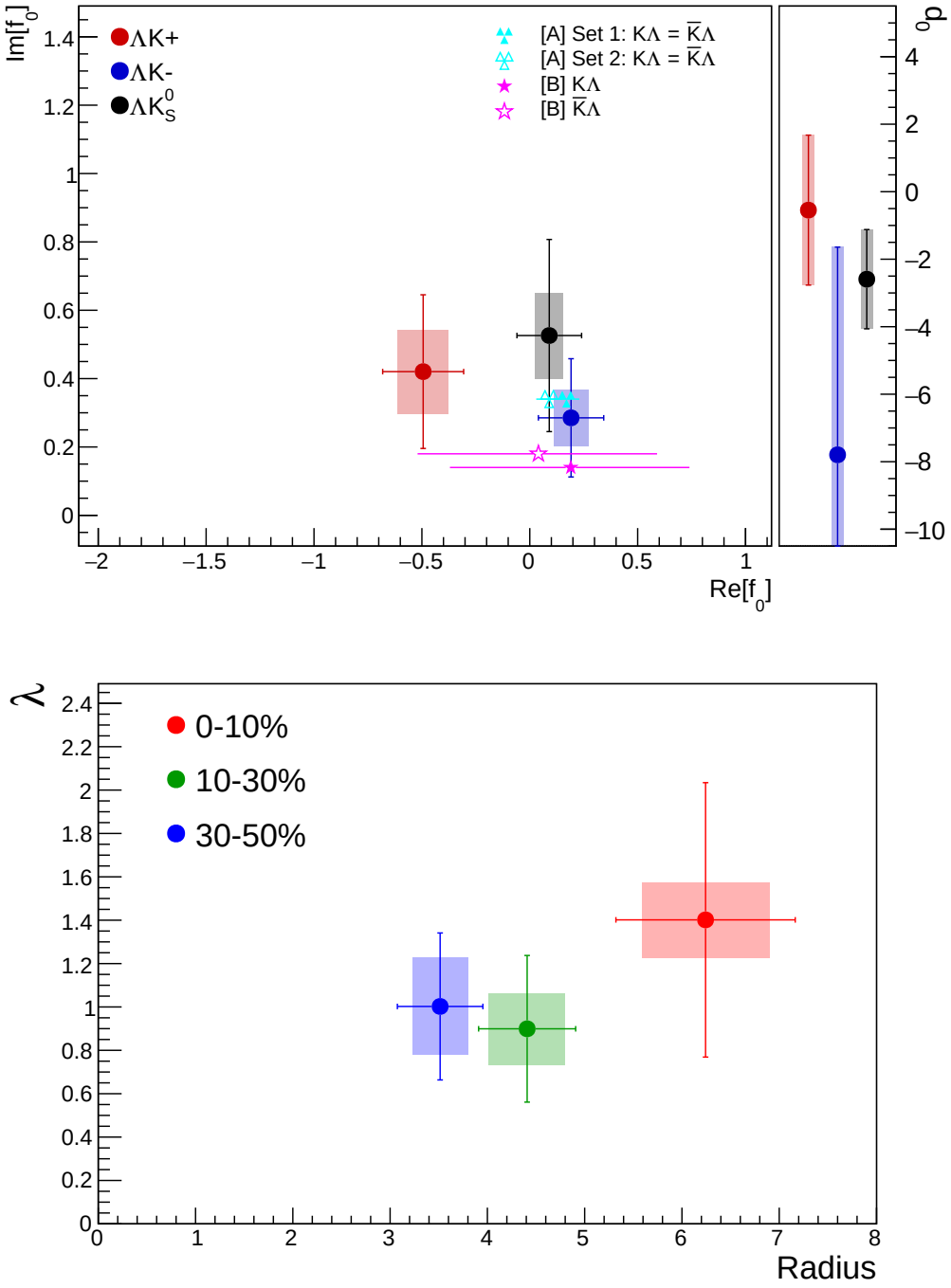

Fig. 1: Extracted fit parameters for the case of 3 residual contributors for all of our ΛK systems. [Top]: $\Im f_0$ vs. $\Re f_0$, together with d_0 to the right. [Bottom]: λ vs. Radius for the 0-10% (blue), 10-30% (green), and 30-50% (red) centrality bins. In the fit, all ΛK systems share common radii. The color scheme used in the panel are to be consistent with those in Fig. 3. The cyan ([A] = Ref. [**?**]) and magenta ([B] = Ref. [**?**]) points show theoretical predictions made using chiral perturbation theory.

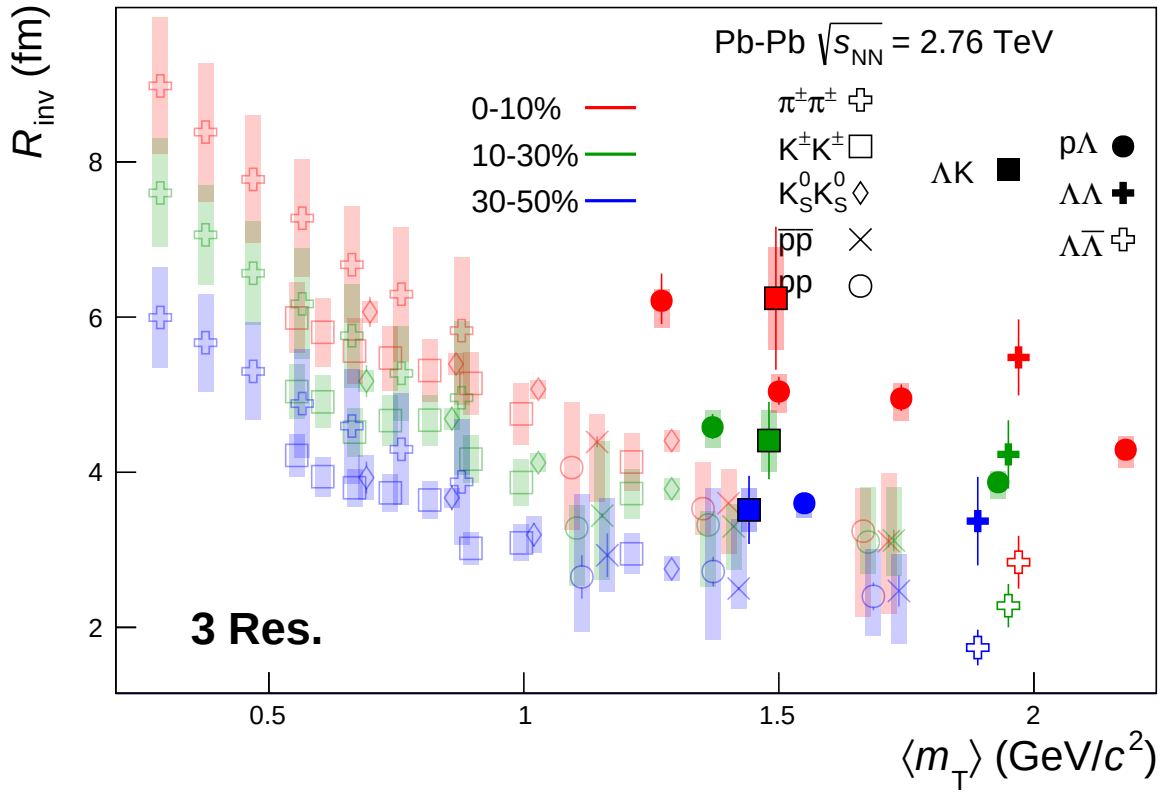

Fig. 2: 3 residual correlations in ΛK fits. Extracted fit $R_{\rm inv}$ parameters as a function of pair transverse mass ($m_{\rm T}$) for various pair systems over several centralities. The ALICE published data [**?**] are shown with transparent, open symbols. The new ΛK results are shown with opaque, filled symbols. The $m_{\rm T}$ value for the ΛK system is an average of those for the ΛK^+, $\bar{\Lambda} K^-$, and ΛK^0_S systems.

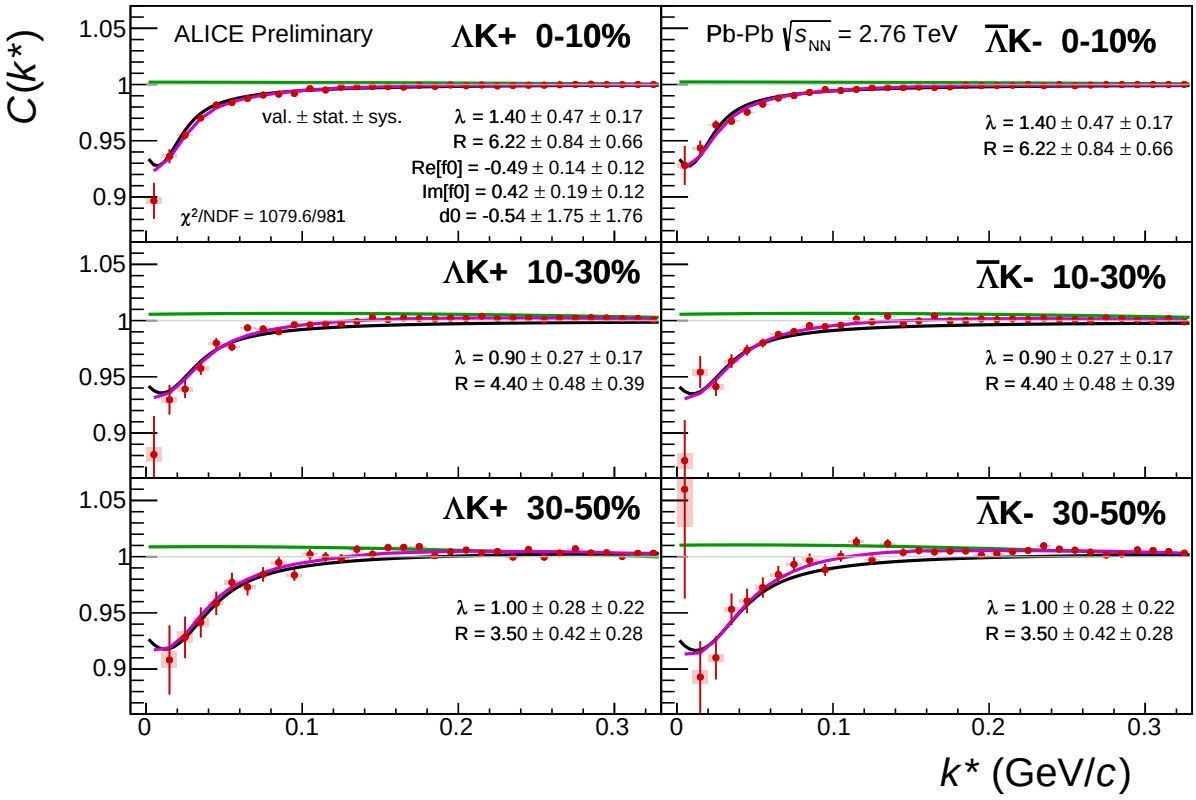

Fig. 3: Fit results, with 3 residual correlations included, for the ΛK^+ and $\bar{\Lambda} K^-$ data. The ΛK^+ data is shown in the left column, the $\bar{\Lambda} K^-$ in the right, and the rows differentiate the different centrality bins (0-10% in the top, 10-30% in the middle, and 30-50% in the bottom). See text for further details.

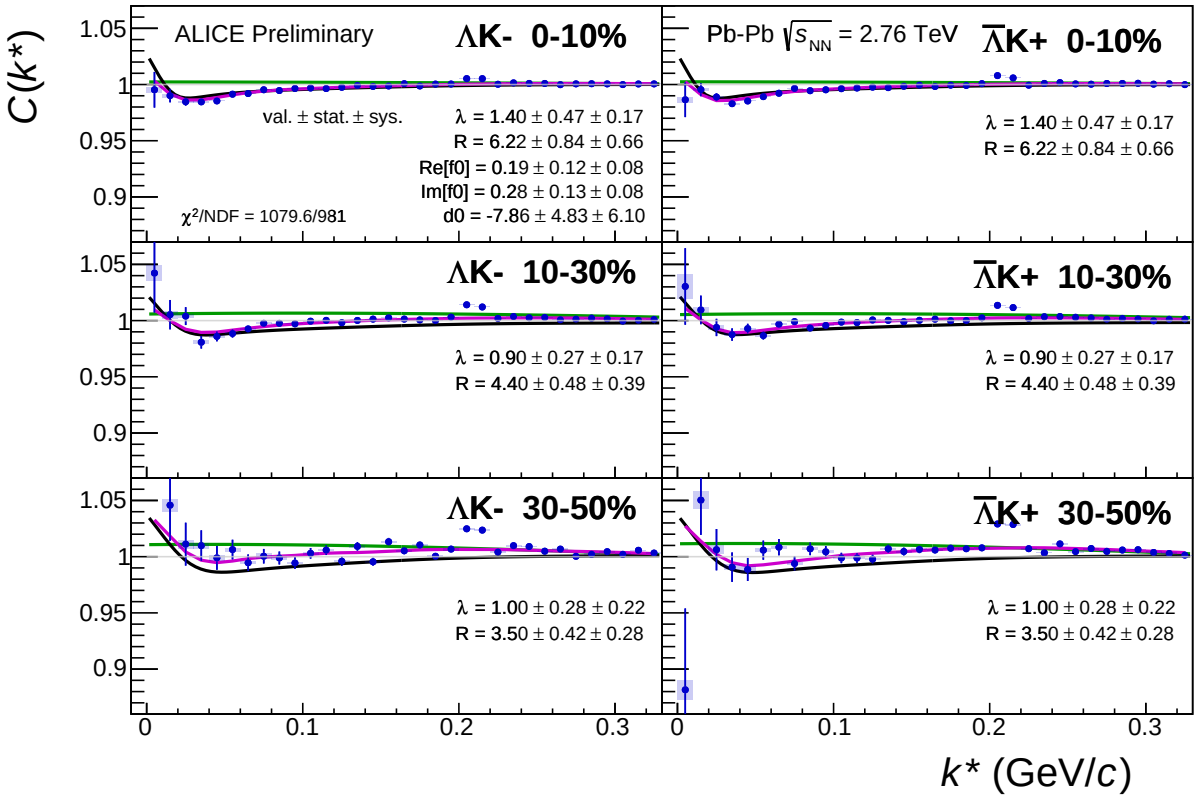

Fig. 4: Fit results, with 3 residual correlations included, for the ΛK^- and $\bar{\Lambda} K^+$ data. The ΛK^- data is shown in the left column, the $\bar{\Lambda} K^+$ in the right, and the rows differentiate the different centrality bins (0-10% in the top, 10-30% in the middle, and 30-50% in the bottom). See text for further details.

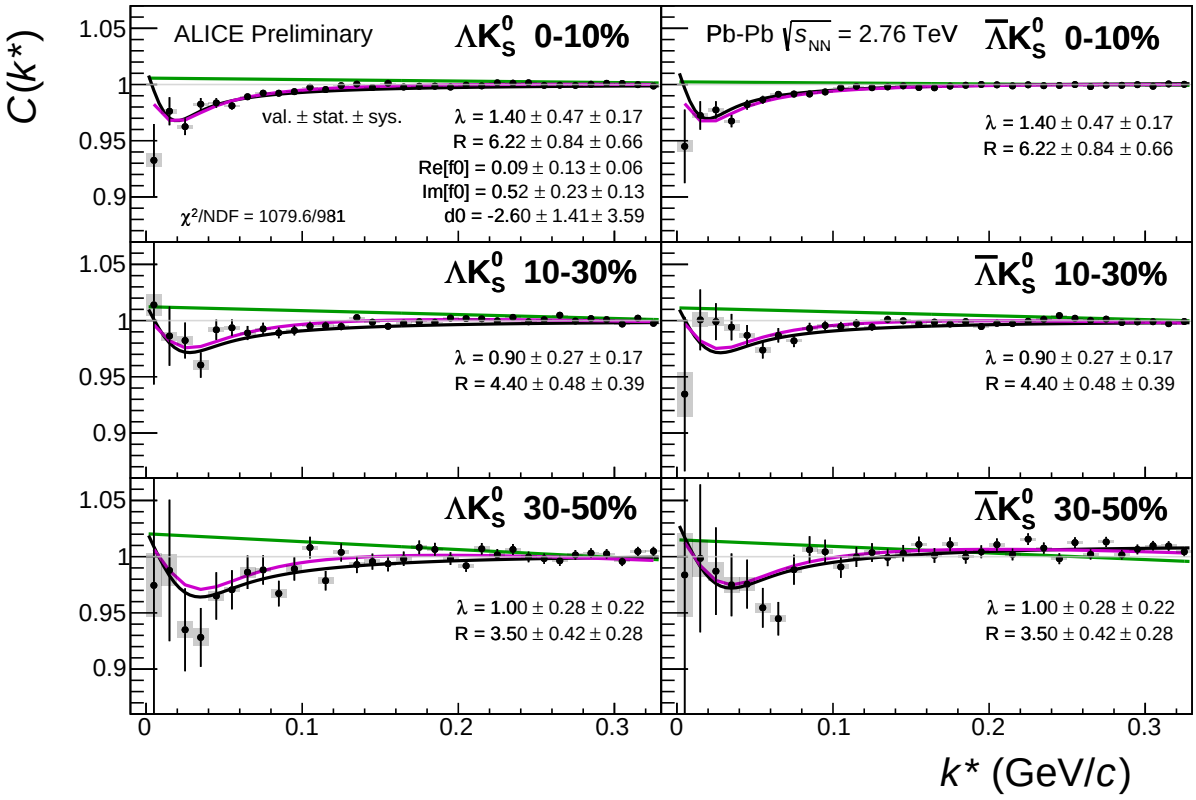

Fig. 5: Fit results, with 3 residual correlations included, for the ΛK^0_S and $\bar{\Lambda} K^0_S$ data. The ΛK^0_S data is shown in the left column, the $\bar{\Lambda} K^0_S$ in the right, and the rows differentiate the different centrality bins (0-10% in the top, 10-30% in the middle, and 30-50% in the bottom). See text for further details.

1.1.2 10 Residual Correlations Included in Fit

Figure 9 nicely collects and summarizes all of our extracted fit parameters for the case of 10 included residual contributors. Figure 10 presents our extracted fit radii, along with those of other systems previously analyzed by ALICE [**?**], as a function of pair transverse mass (m_{T}). Figures 11, 12, and 13 show the experimental correlation functions with fits, assuming 10 residual contributors, for all studied centralities for $\Lambda\mathrm{K}^0_{\mathrm{S}}$ with $\bar{\Lambda}\mathrm{K}^0_{\mathrm{S}}$, $\Lambda\mathrm{K}^+$ with $\bar{\Lambda}\mathrm{K}^-$, and $\Lambda\mathrm{K}^-$ with $\bar{\Lambda}\mathrm{K}^+$, respectively. The parameter sets extracted from the fits can be found in Tables **??** and **??**.

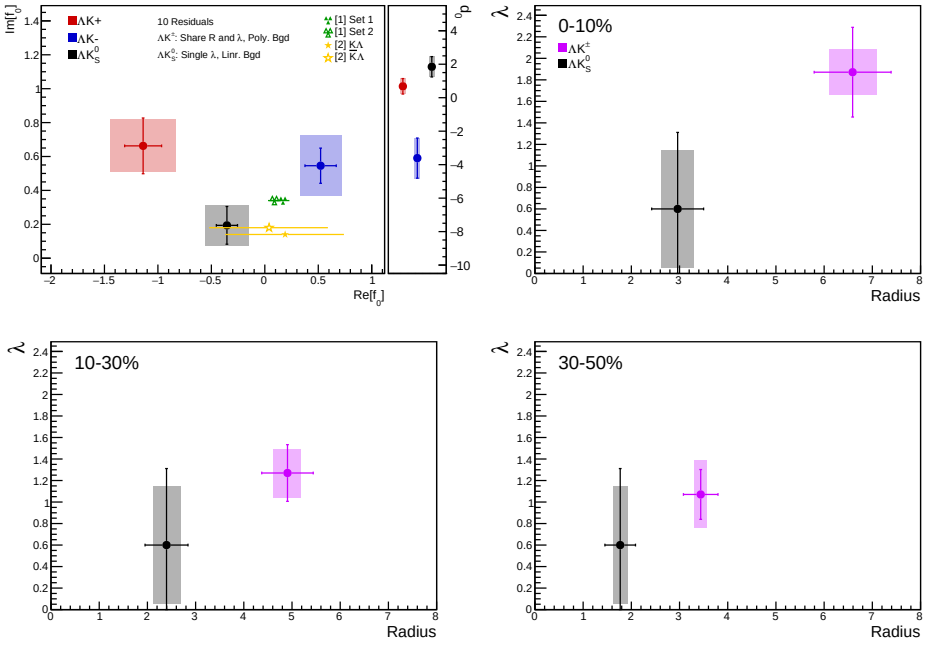

Fig. 6: Extracted scattering parameters for the case of 10 residual contributors for all of our ΛK systems. [Top Left]: $\Im f_0$ vs. $\Re f_0$, together with d_0 to the right. [Top Right (Bottom Left, Bottom Right)]: λ vs. Radius for the 0-10% (10-30%, 30-50%) bin. The green [**?**] and yellow [**?**] points show theoretical predictions made using chiral perturbation theory.

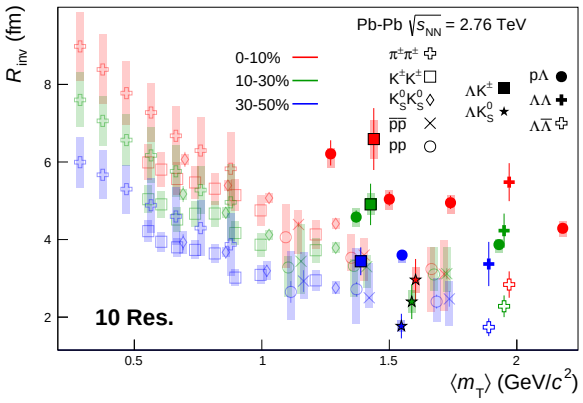

Fig. 7: 10 residual correlations in ΛK fits. Extracted fit R_{inv} parameters as a function of pair transverse mass (m_{T}) for various pair systems over several centralities. The ALICE published data [**?**] is shown with transparent, open symbols. The new ΛK results are shown with opaque, filled symbols. In the left, the $\Lambda\mathrm{K}^+$ (with it's conjugate pair) results are shown separately from the $\Lambda\mathrm{K}^-$ (with it's conjugate pair) results. In the right, all $\Lambda\mathrm{K}^{\pm}$ results are averaged.

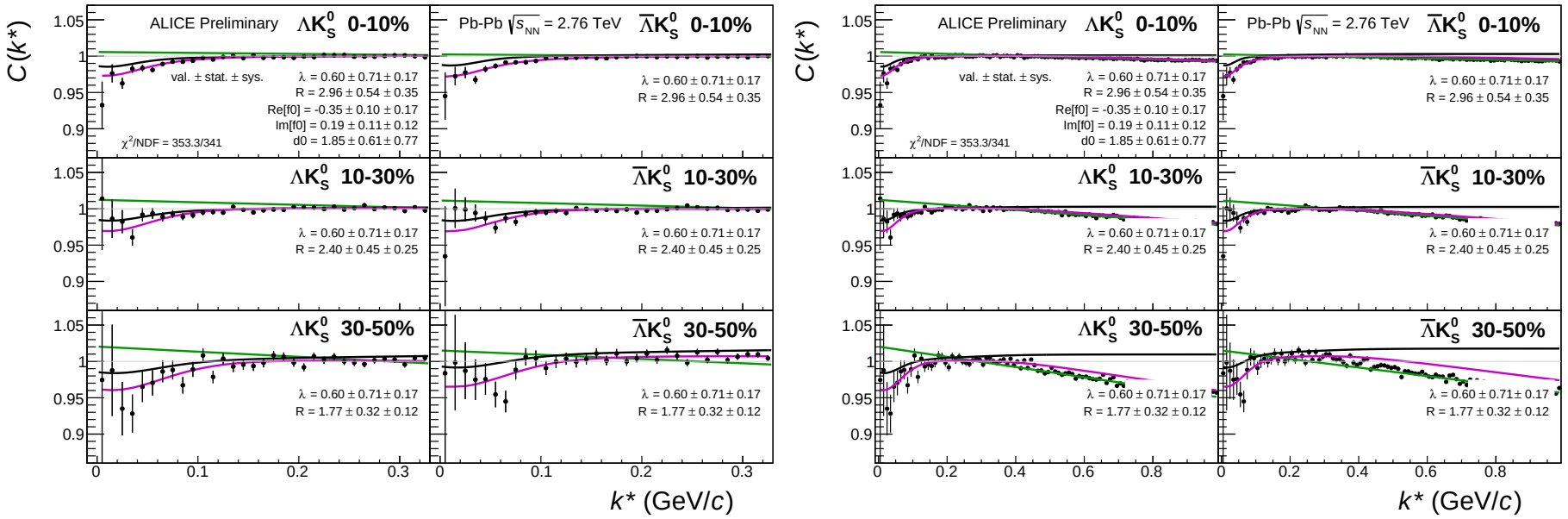

(a) Signal region view ($k^* \lesssim 0.3$ GeV/c)

(b) Wide view ($k^* \lesssim 1.0$ GeV/c)

Fig. 8: Fits, with 10 residual correlations included, to the ΛK^0_S (left) and $\bar{\Lambda} K^0_S$ (right) data for the centralities 0-10% (top), 10-30% (middle), and 30-50% (bottom). The lines represent the statistical errors, while the boxes represent the systematic errors. A single λ parameter is shared amongst all. Each analysis has a unique normalization parameter. The radii are shared between analyses of like centrality, as these should have similar source sizes. The scattering parameters ($\Im f_0$, $\Re f_0$, d_0) are shared amongst all. The background is modeled by a (6^{th}-)degree polynomial fit to THERMINATOR simulation. The black solid line represents the primary (ΛK) correlation's contribution to the fit. The green line shows the fit to the non-flat background. The purple points show the fit after all residuals' contributions have been included, and momentum resolution and non-flat background corrections have been applied. The extracted fit values with uncertainties are printed.

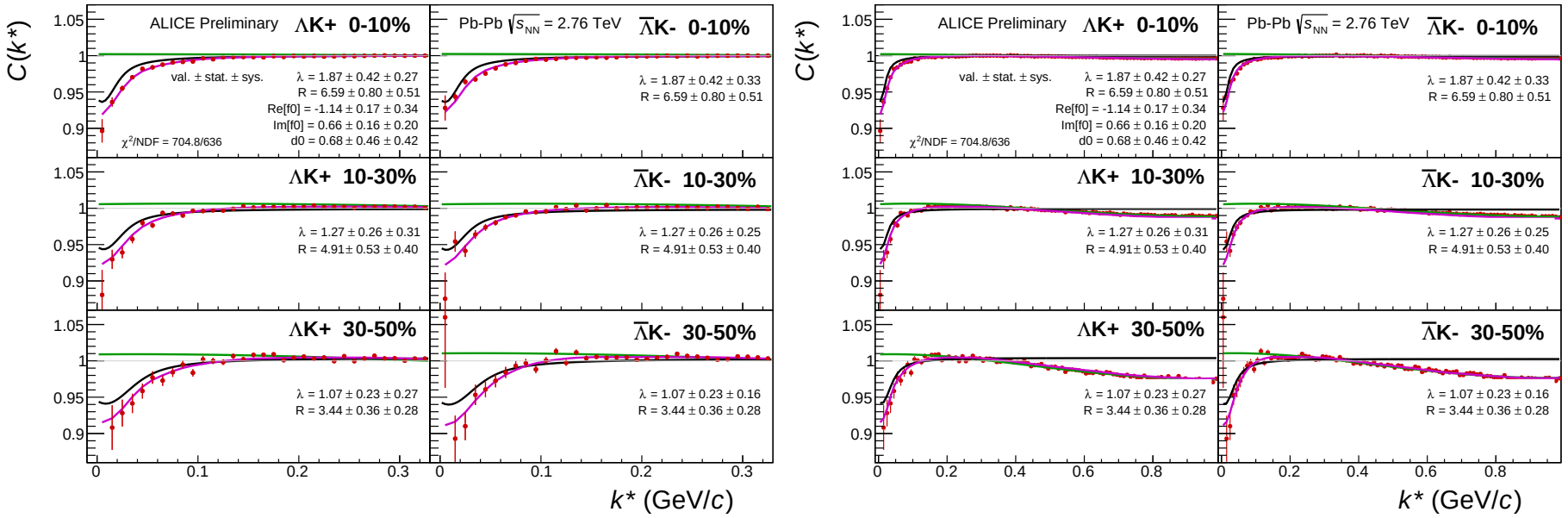

(a) Signal region view ($k^* \lesssim 0.3$ GeV/c)

(b) Wide view ($k^* \lesssim 1.0$ GeV/c)

Fig. 9: Fits, with 10 residual correlations included, to the ΛK^+ (left) and $\bar{\Lambda} K^-$ (right) data for the centralities 0-10% (top), 10-30% (middle), and 30-50% (bottom). The lines represent the statistical errors, while the boxes represent the systematic errors. All $\Lambda K^{\pm}$ analyses are fit simultaneously across all centralities (0-10%, 10-30%, 30-50%). Scattering parameters ($\Im f_0$, $\Re f_0$, d_0) are shared between pair-conjugate systems (i.e. a parameter set describing the ΛK^+ & $\bar{\Lambda} K^-$ system, and a separate set describing the ΛK^- & $\bar{\Lambda} K^+$ system). For each centrality, a radius and λ parameters are shared between all pairs (ΛK^+, $\bar{\Lambda} K^-$, ΛK^-, $\bar{\Lambda} K^+$). Each analysis has a unique normalization parameter. The background is modeled by a (6^{th}-)degree polynomial fit to THERMINATOR simulation. The black solid line represents the primary (ΛK) correlation's contribution to the fit. The green line shows the fit to the non-flat background. The purple points show the fit after all residuals' contributions have been included, and momentum resolution and non-flat background corrections have been applied. The extracted fit values with uncertainties are printed.

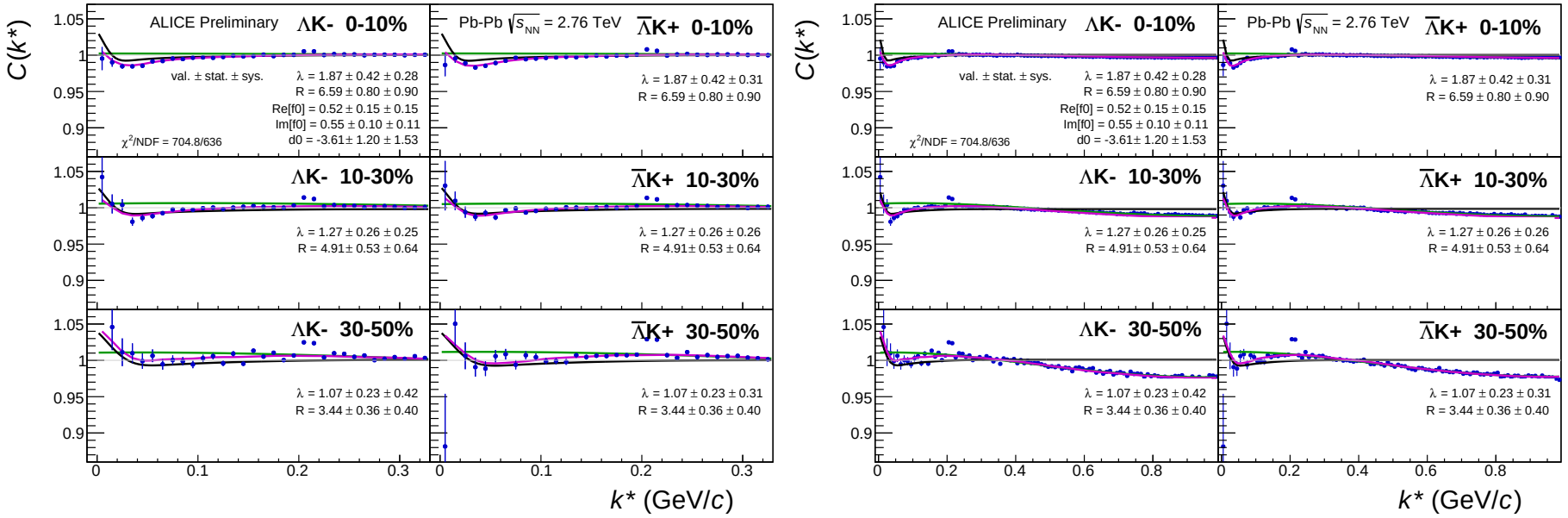

(a) Signal region view ($k^* \lesssim 0.3$ GeV/c)

(b) Wide view ($k^* \lesssim 1.0$ GeV/c)

Fig. 10: Fits, with 10 residual correlations included, to the ΛK^-(left) with $\bar{\Lambda}K^+$ (right) data for the centralities 0-10% (top), 10-30% (middle), and 30-50% (bottom). The lines represent the statistical errors, while the boxes represent the systematic errors. All $\Lambda K^{\pm}$ analyses are fit simultaneously across all centralities (0-10%, 10-30%, 30-50%). Scattering parameters ($\Im f_0$, $\Re f_0$, d_0) are shared between pair-conjugate systems (i.e. a parameter set describing the ΛK^+ & $\bar{\Lambda}K^-$ system, and a separate set describing the ΛK^- & $\bar{\Lambda}K^+$ system). For each centrality, a radius and λ parameters are shared between all pairs (ΛK^+, $\bar{\Lambda}K^-$, ΛK^-, $\bar{\Lambda}K^+$). Each analysis has a unique normalization parameter. The background is modeled by a (6^{th}-)degree polynomial fit to THERMINATOR simulation. The black solid line represents the primary (ΛK) correlation's contribution to the fit. The green line shows the fit to the non-flat background. The purple points show the fit after all residuals' contributions have been included, and momentum resolution and non-flat background corrections have been applied. The extracted fit values with uncertainties are printed.

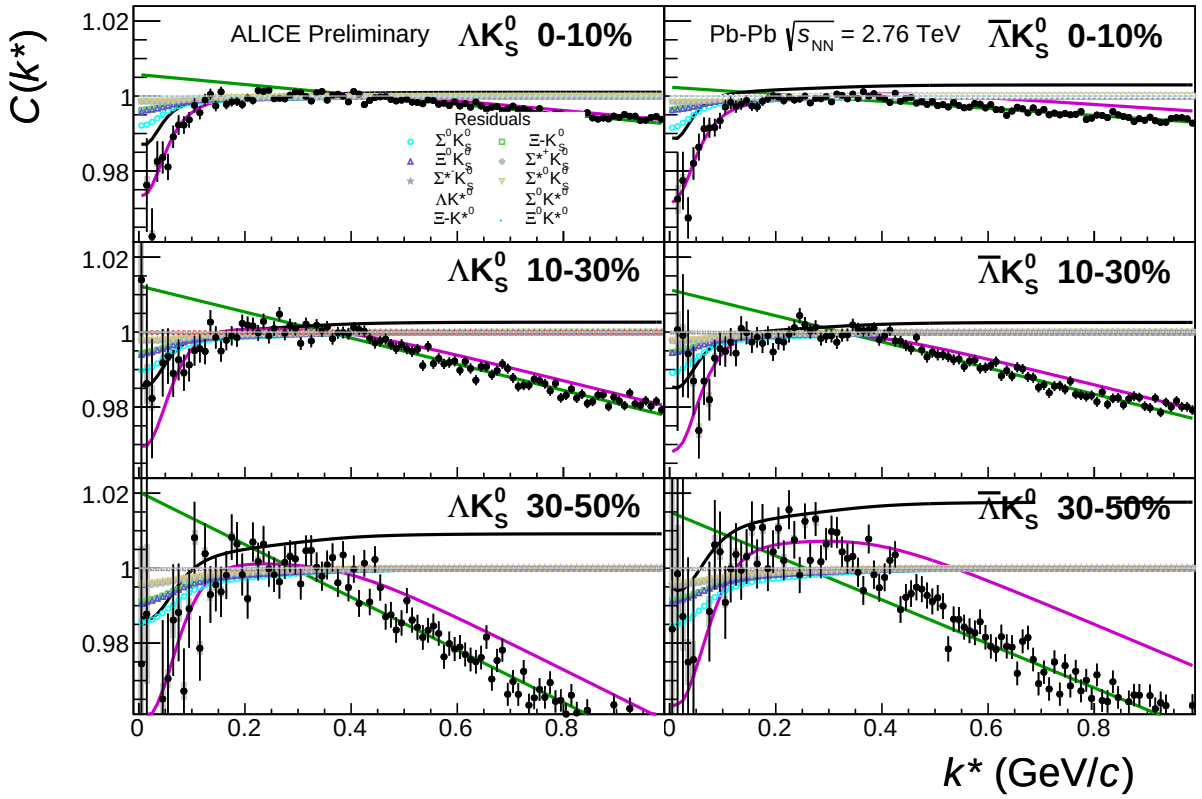

Fig. 11: Fits, with 10 residual correlations included and shown, to the ΛK^0_S (left) and $\bar{\Lambda}K^0_S$ (right) data for the centralities 0-10% (top), 10-30% (middle), and 30-50% (bottom). The ten parent pairs used for the residual correction to the ΛK^0_S ($\bar{\Lambda}K^0_S$) fit are $\Sigma^0K^0_S$, $\Xi^0K^0_S$, $\Xi^-K^0_S$, $\Sigma^{*(+,-,0)}K^0_S$, ΛK^{*0}, Σ^0K^{*0}, Ξ^0K^{*0}, and Ξ^-K^{*0} ($\bar{\Sigma}^0K^0_S$, $\bar{\Xi}^0K^0_S$, $\bar{\Xi}^+K^0_S$, $\bar{\Sigma}^{*(+,-,0)}K^0_S$, $\bar{\Lambda}\bar{K}^{*0}$, $\bar{\Sigma}^0\bar{K}^{*0}$, $\bar{\Xi}^0\bar{K}^{*0}$, and $\bar{\Xi}^+\bar{K}^{*0}$).

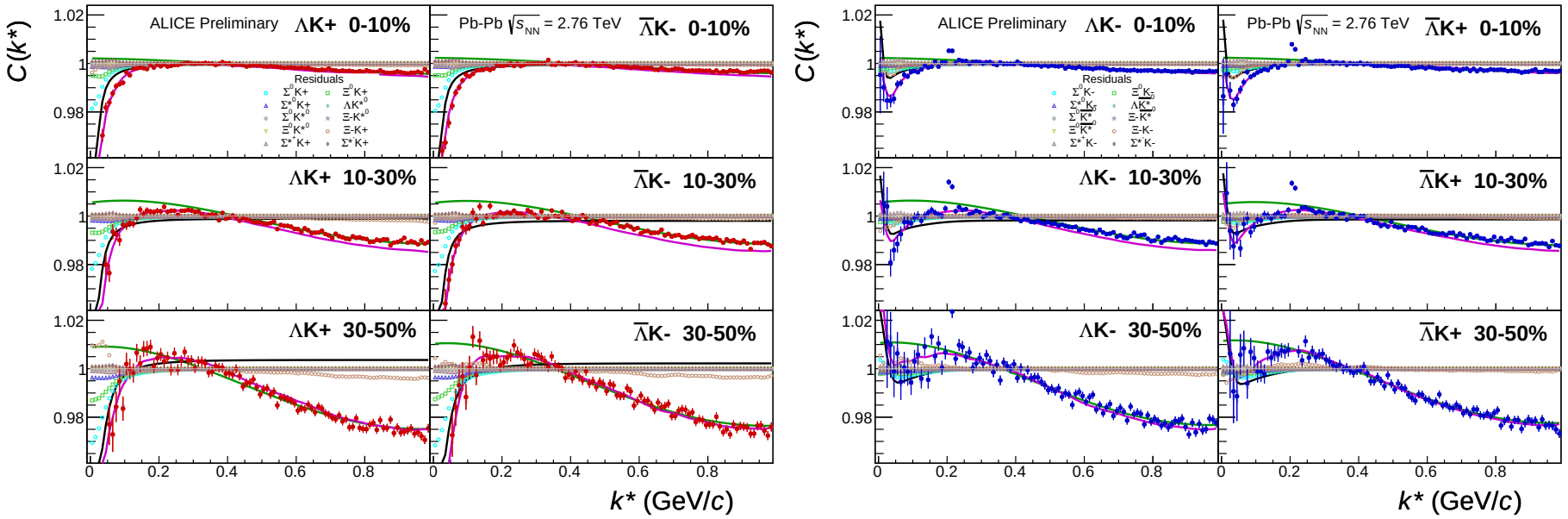

(a) $\Lambda K^{+}(\bar{\Lambda}K^{-})$ fits with residual contributions shown for the centralities 0-10% (top), 10-30% (middle), and 30-50% (bottom)

(b) $\Lambda K^{-}(\bar{\Lambda}K^{+})$ fits with residual contributions shown for the centralities 0-10% (top), 10-30% (middle), and 30-50% (bottom)

Fig. 12: Fits, with 10 residual correlations included and shown, to the ΛK^{+} & $\bar{\Lambda}K^{-}$ (left) and ΛK^{-} & $\bar{\Lambda}K^{+}$ (right) data for the centralities 0-10% (top), 10-30% (middle), and 30-50% (bottom). The ten parent pairs used for the residual correction to the ΛK^{+} ($\bar{\Lambda}K^{-}$) fit are $\Sigma^{0}K^{+}$, $\Xi^{0}K^{+}$, $\Xi^{-}K^{+}$, $\Sigma^{*(+,-,0)}K^{+}$, ΛK^{*0}, $\Sigma^{0}K^{*0}$, $\Xi^{0}K^{*0}$, and $\Xi^{-}K^{*0}$ ($\bar{\Sigma}^{0}K^{-}$, $\bar{\Xi}^{0}K^{-}$, $\bar{\Xi}^{+}K^{-}$, $\bar{\Sigma}^{*(+,-,0)}K^{-}$, $\bar{\Lambda}\bar{K}^{*0}$, $\bar{\Sigma}^{0}\bar{K}^{*0}$, $\bar{\Xi}^{0}\bar{K}^{*0}$, and $\bar{\Xi}^{+}\bar{K}^{*0}$).

Fit Results $\Lambda(\bar{\Lambda})K^0_S$

System	Centrality	Fit Parameters				
		λ	R	$\mathbb{R}f_0$	$\mathbb{I}f_0$	d_0
ΛK^0_S & $\bar{\Lambda}K^0_S$	0-10%	0.60 ± 0.71 (stat.) ± 0.54 (sys.)	2.96 ± 0.54 (stat.) ± 0.33 (sys.)	-0.35 ± 0.10 (stat.) ± 0.21 (sys.)	0.19 ± 0.11 (stat.) ± 0.12 (sys.)	1.85 ± 0.61 (stat.) ± 2.68 (sys.)
	10-30%		2.40 ± 0.45 (stat.) ± 0.29 (sys.)			
	30-50%		1.77 ± 0.32 (stat.) ± 0.15 (sys.)			

Table 2: Fit Results $\Lambda(\bar{\Lambda})K^0_S$, with 10 residual correlations included. Each pair is fit simultaneously with its conjugate (ie. ΛK^0_S with $\bar{\Lambda}K^0_S$) across all centralities (0-10%, 10-30%, 30-50%), for a total of 6 simultaneous analyses in the fit. A single λ parameter is shared amongst all. Each analysis has a unique normalization parameter. The radii are shared between analyses of like centrality, as these should have similar source sizes. The scattering parameters ($\mathbb{R}f_0$, $\mathbb{I}f_0$, d_0) are shared amongst all. The background is fit with a linear form in the range $0.6 < k^* < 0.9$ GeV/c. The fit is done on the data with only statistical error bars. The errors marked as "stat." are those returned by MINUIT. The errors marked as "sys." are those which result from my systematic analysis (as outlined in Section **??**).

Fit Results $\Lambda(\bar{\Lambda})K^{\pm}$

System	Centrality	Fit Parameters				
		λ	R	$\mathbb{R}f_0$	$\mathbb{I}f_0$	d_0
ΛK^+ & $\bar{\Lambda}K^-$	0-10%	1.87 ± 0.42 (stat.) ± 0.21 (sys.)	6.59 ± 0.80 (stat.) ± 0.49 (sys.)	-1.14 ± 0.17 (stat.) ± 0.31 (sys.)	0.66 ± 0.16 (stat.) ± 0.15 (sys.)	0.68 ± 0.46 (stat.) ± 0.53 (sys.)
	10-30%	1.27 ± 0.26 (stat.) ± 0.23 (sys.)	4.91 ± 0.53 (stat.) ± 0.28 (sys.)			
ΛK^+ & $\bar{\Lambda}K^-$	30-50%	1.07 ± 0.23 (stat.) ± 0.32 (sys.)	3.44 ± 0.36 (stat.) ± 0.13 (sys.)	0.52 ± 0.15 (stat.) ± 0.19 (sys.)	0.55 ± 0.10 (stat.) ± 0.18 (sys.)	-3.61 ± 1.20 (stat.) ± 1.02 (sys.)

Table 3: Fit Results $\Lambda(\bar{\Lambda})K^{\pm}$, with 10 residual correlations included. All $\Lambda K^{\pm}$ analyses are fit simultaneously across all centralities (0-10%, 10-30%, 30-50%). Scattering parameters ($\mathbb{R}f_0$, $\mathbb{I}f_0$, d_0) are shared between pair-conjugate systems (i.e. a parameter set describing the ΛK^+ & $\bar{\Lambda}K^-$ system, and a separate set describing the ΛK^- & $\bar{\Lambda}K^+$ system). For each centrality, a radius and λ parameters are shared between all pairs (ΛK^+, $\bar{\Lambda}K^-$, ΛK^-, $\bar{\Lambda}K^+$). Each analysis has a unique normalization parameter. The background is modeled by a (6^{th}-)degree polynomial fit to THERMINATOR simulation. The fit is done on the data with only statistical error bars. The errors marked as "stat." are those returned by MINUIT. The errors marked as "sys." are those which result from my systematic analysis (as outlined in Section **??**).

1.1.3 No Residual Correlations Included in Fit

Figure 16 nicely collects and summarizes all of our extracted fit parameters for the case of no included residual contributors. Figure 17 presents our extracted fit radii, along with those of other systems previously analyzed by ALICE [**?**], as a function of pair transverse mass (m_{T}). Figures 18, 19, and 20 show the experimental correlation functions with fits, assuming no residual contributors, for all studied centralities for $\Lambda\mathrm{K}^0_{\mathrm{S}}$ with $\bar{\Lambda}\mathrm{K}^0_{\mathrm{S}}$, $\Lambda\mathrm{K}^+$ with $\bar{\Lambda}\mathrm{K}^-$, and $\Lambda\mathrm{K}^-$ with $\bar{\Lambda}\mathrm{K}^+$, respectively. The parameter sets extracted from the fits can be found in Tables 5 and 6.

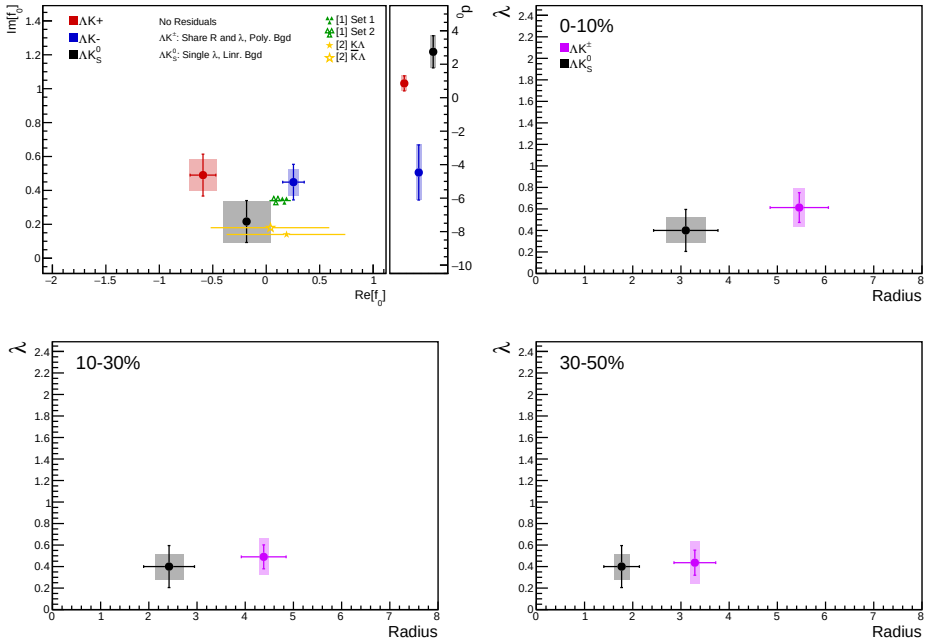

Fig. 13: Extracted scattering parameters for the case of NO residual contributors for all of our ΛK systems. [Top Left]: $\Im f_0$ vs. $\Re f_0$, together with d_0 to the right. [Top Right (Bottom Left, Bottom Right)]: λ vs. Radius for the 0-10% (10-30%, 30-50%) bin. The green [**?**] and yellow [**?**] points show theoretical predictions made using chiral perturbation theory.

Figure 17 shows extracted R_{inv} parameters as a function of tranverse mass (m_{T}) for various pair systems over several centralities. The published ALICE data [**?**] is shown with transparent, open symbols. The new ΛK results are shown with opaque, filled symbols. The radii shown an increasing size with increasing centrality, as is expected from the simple geometric picture of the collisions. The radii decrease in size with increasing m_{T}, and we see an approximate scaling of the radii with transverse mass, as is expected in the presence of collective flow in the system.

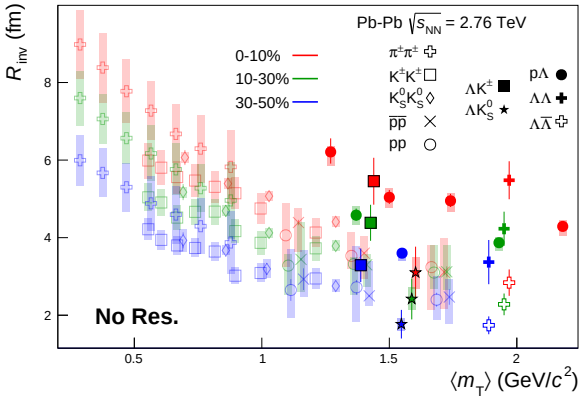

Fig. 14: No residual correlations in ΛK fits. Extracted fit R_{inv} parameters as a function of pair transverse mass (m_{T}) for various pair systems over several centralities. The ALICE published data [**?**] is shown with transparent, open symbols. The new ΛK results are shown with opaque, filled symbols. In the left, the ΛK^{+} (with it's conjugate pair) results are shown separately from the ΛK^{-} (with it's conjugate pair) results. In the right, all $\Lambda K^{\pm}$ results are averaged.

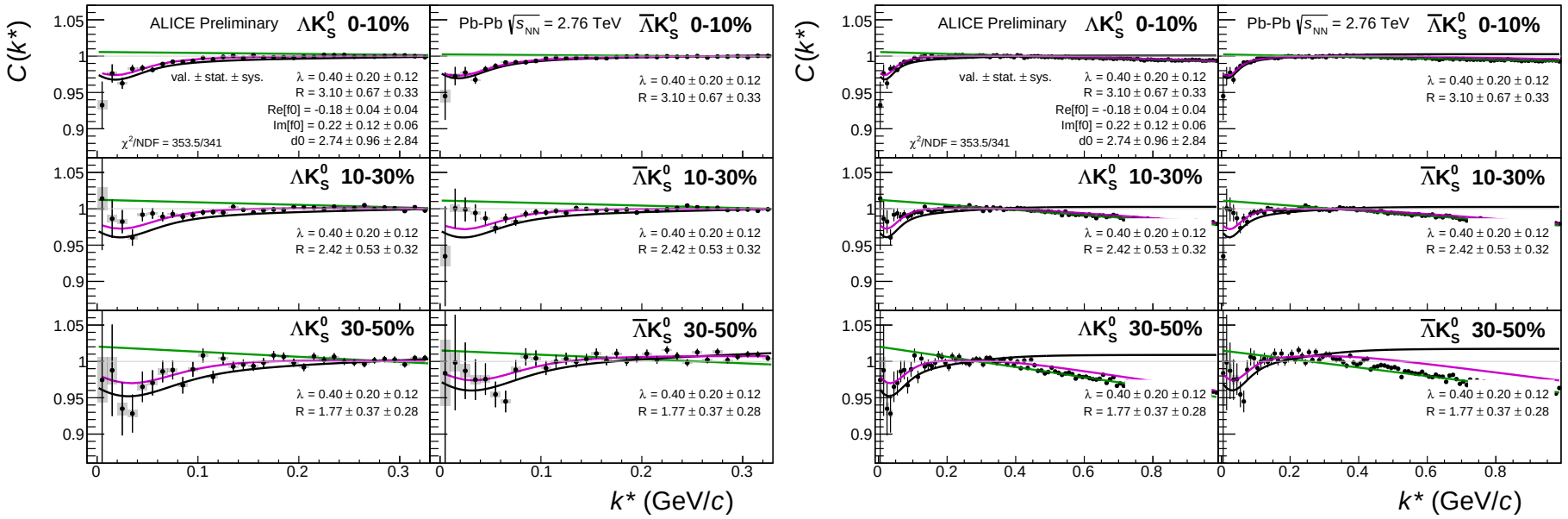

(a) Signal region view ($k^* \lesssim 0.3$ GeV/c)

(b) Wide view ($k^* \lesssim 1.0$ GeV/c)

Fig. 15: Fits, with NO residual correlations included, to the ΛK^0_S (left) and $\bar{\Lambda} K^0_S$ (right) data for the centralities 0-10% (top), 10-30% (middle), and 30-50% (bottom). The lines represent the statistical errors, while the boxes represent the systematic errors. A single λ parameter is shared amongst all. Each analysis has a unique normalization parameter. The radii are shared between analyses of like centrality, as these should have similar source sizes. The scattering parameters ($\Im f_0$, $\Re f_0$, d_0) are shared amongst all. The background is modeled by a (6^{th}-)degree polynomial fit to THERMINATOR simulation. The black solid line represents the "raw" primary fit, i.e. not corrected for momentum resolution effects nor non-flat background. The green line shows the fit to the non-flat background. The purple points show the fit after momentum resolution and non-flat background corrections have been applied. The extracted fit values with uncertainties are printed.

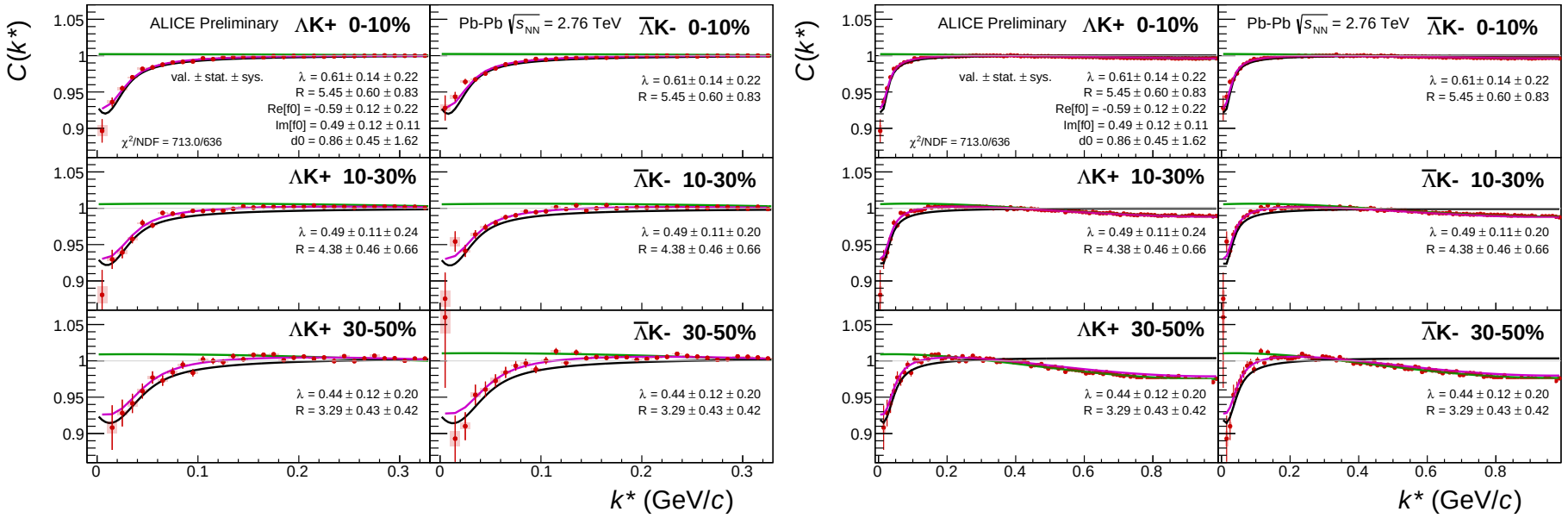

(a) Signal region view ($k^* \lesssim 0.3$ GeV/c)

(b) Wide view ($k^* \lesssim 1.0$ GeV/c)

Fig. 16: Fits to the ΛK^+ (left) and $\bar{\Lambda} K^-$ (right) data for the centralities 0-10% (top), 10-30% (middle), and 30-50% (bottom). The lines represent the statistical errors, while the boxes represent the systematic errors. All $\Lambda K^{\pm}$ analyses are fit simultaneously across all centralities (0-10%, 10-30%, 30-50%). Scattering parameters ($\Im f_0$, $\Re f_0$, d_0) are shared between pair-conjugate systems (i.e. a parameter set describing the ΛK^+ & $\bar{\Lambda} K^-$ system, and a separate set describing the ΛK^- & $\bar{\Lambda} K^+$ system). For each centrality, a radius and λ parameters are shared between all pairs (ΛK^+, $\bar{\Lambda} K^-$, ΛK^-, $\bar{\Lambda} K^+$). Each analysis has a unique normalization parameter. The background is modeled by a (6^{th}-)degree polynomial fit to THERMINATOR simulation. The black solid line represents the "raw" primary fit, i.e. not corrected for momentum resolution effects nor non-flat background. The green line shows the fit to the non-flat background. The purple points show the fit after momentum resolution and non-flat background corrections have been applied. The extracted fit values with uncertainties are printed.

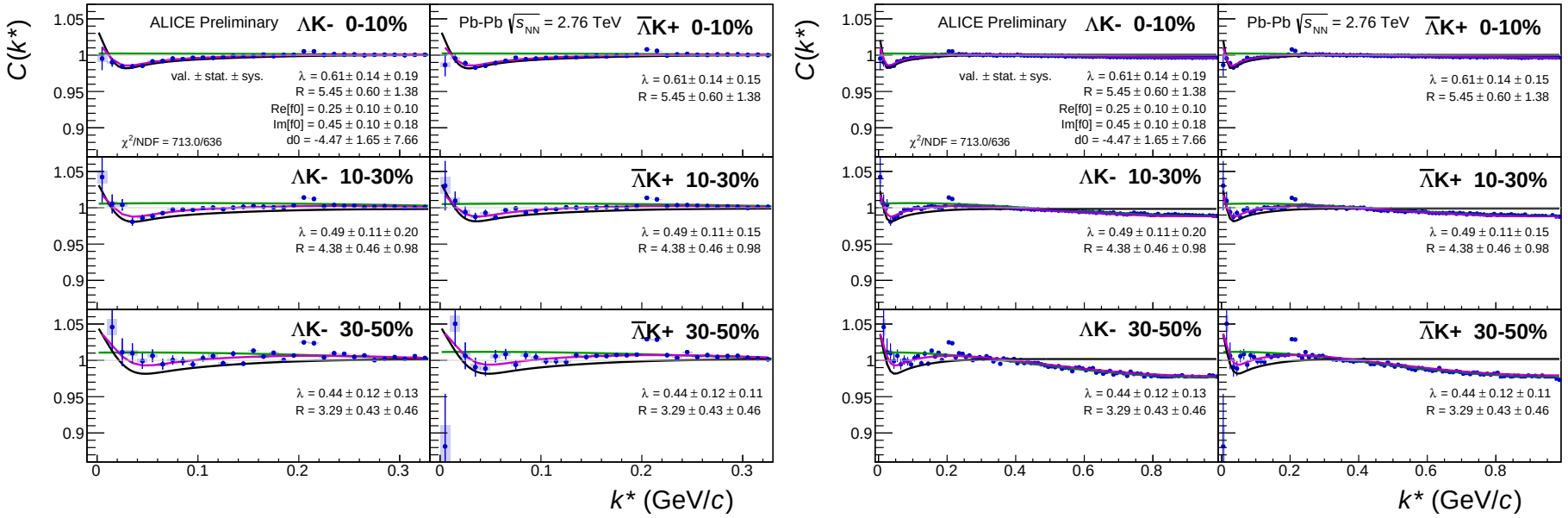

(a) Signal region view ($k^* \lesssim 0.3$ GeV/c)

(b) Wide view ($k^* \lesssim 1.0$ GeV/c)

Fig. 17: Fits, with NO residual correlations included, to the ΛK^-(left) with $\bar{\Lambda}K^+$ (right) data for the centralities 0-10% (top), 10-30% (middle), and 30-50% (bottom). The lines represent the statistical errors, while the boxes represent the systematic errors. All $\Lambda K^{\pm}$ analyses are fit simultaneously across all centralities (0-10%, 10-30%, 30-50%). Scattering parameters ($\Im f_0$, $\Re f_0$, d_0) are shared between pair-conjugate systems (i.e. a parameter set describing the ΛK^+ & $\bar{\Lambda}K^-$ system, and a separate set describing the ΛK^- & $\bar{\Lambda}K^+$ system). For each centrality, a radius and λ parameters are shared between all pairs (ΛK^+, $\bar{\Lambda}K^-$, ΛK^-, $\bar{\Lambda}K^+$). Each analysis has a unique normalization parameter. The background is modeled by a (6^{th}-)degree polynomial fit to THERMINATOR simulation. The black solid line represents the "raw" primary fit, i.e. not corrected for momentum resolution effects nor non-flat background. The green line shows the fit to the non-flat background. The purple points show the fit after momentum resolution and non-flat background corrections have been applied. The extracted fit values with uncertainties are printed.

Fit Results $\Lambda(\bar{\Lambda})K^0_S$

System	Centrality	Fit Parameters				
		λ	R	$\mathbb{R}f_0$	$\mathbb{I}f_0$	d_0
ΛK^0_S & $\bar{\Lambda}K^0_S$	0-10%	0.40 ± 0.20 (stat.) ± 0.12 (sys.)	3.10 ± 0.67 (stat.) ± 0.41 (sys.)	-0.18 ± 0.04 (stat.) ± 0.22 (sys.)	0.22 ± 0.12 (stat.) ± 0.12 (sys.)	2.74 ± 0.96 (stat.) ± 1.28 (sys.)
	10-30%		2.42 ± 0.53 (stat.) ± 0.29 (sys.)			
	30-50%		1.77 ± 0.37 (stat.) ± 0.16 (sys.)			

Table 4: Fit Results $\Lambda(\bar{\Lambda})K^0_S$, with no residual correlations included. Each pair is fit simultaneously with its conjugate (ie. ΛK^0_S with $\bar{\Lambda}K^0_S$) across all centralities (0-10%, 10-30%, 30-50%), for a total of 6 simultaneous analyses in the fit. A single λ parameter is shared amongst all. Each analysis has a unique normalization parameter. The radii are shared between analyses of like centrality, as these should have similar source sizes. The scattering parameters ($\mathbb{R}f_0$, $\mathbb{I}f_0$, d_0) are shared amongst all. The background is fit with a linear form in the range $0.6 < k^* < 0.9$ GeV/c. The fit is done on the data with only statistical error bars. The errors marked as "stat." are those returned by MINUIT. The errors marked as "sys." are those which result from my systematic analysis (as outlined in Section **??**).

Fit Results $\Lambda(\bar{\Lambda})K^{\pm}$

System	Centrality	Fit Parameters				
		λ	R	$\mathbb{R}f_0$	$\mathbb{I}f_0$	d_0
ΛK^+ & $\bar{\Lambda}K^-$	0-10%	0.61 ± 0.14 (stat.) ± 0.18 (sys.)	5.45 ± 0.60 (stat.) ± 0.12 (sys.)	-0.59 ± 0.12 (stat.) ± 0.13 (sys.)	0.49 ± 0.12 (stat.) ± 0.09 (sys.)	0.86 ± 0.45 (stat.) ± 1.63 (sys.)
	10-30%	0.49 ± 0.11 (stat.) ± 0.17 (sys.)	4.38 ± 0.46 (stat.) ± 0.10 (sys.)			
ΛK^+ & $\bar{\Lambda}K^-$	30-50%	0.44 ± 0.12 (stat.) ± 0.20 (sys.)	3.29 ± 0.43 (stat.) ± 0.10 (sys.)	0.25 ± 0.10 (stat.) ± 0.05 (sys.)	0.45 ± 0.10 (stat.) ± 0.08 (sys.)	-4.47 ± 1.65 (stat.) ± 1.60 (sys.)

Table 5: Fit Results $\Lambda(\bar{\Lambda})K^{\pm}$, with no residual correlations included. All $\Lambda K^{\pm}$ analyses are fit simultaneously across all centralities (0-10%, 10-30%, 30-50%). Scattering parameters ($\mathbb{R}f_0$, $\mathbb{I}f_0$, d_0) are shared between pair-conjugate systems (i.e. a parameter set describing the ΛK^+ & $\bar{\Lambda}K^-$ system, and a separate set describing the ΛK^- & $\bar{\Lambda}K^+$ system). For each centrality, a radius and λ parameters are shared between all pairs (ΛK^+, $\bar{\Lambda}K^-$, ΛK^-, $\bar{\Lambda}K^+$). Each analysis has a unique normalization parameter. The background is modeled by a (6^{th}-)degree polynomial fit to THERMINATOR simulation. The fit is done on the data with only statistical error bars. The errors marked as "stat." are those returned by MINUIT. The errors marked as "sys." are those which result from my systematic analysis (as outlined in Section **??**).

1.1.4 Fit Method Comparisons

The figures in this appendix show comparisons of extracted fit parameters obtained using different fit techniques. Fig. **??** shows a comparison of results obtained using three, ten, and no residual contributors. In Fig. **??**, we demonstrate the effect of fixing the overall $\lambda_{\rm Fit}$ parameter compared to allowing it to be free (see Eq. **??** in Sec. **??**). Fig. **??** compares our normal fit results to those obtained when the correlation functions are built using the Stavinskiy method (see Sec. **??**). Fig. **??** shows the difference between sharing radii among all ΛK systems versus only sharing radii between the $\Lambda K^{\pm}$ systems. Finally, Fig. **??** shows the effect of using the experimental $\Xi^{-}K^{\pm}$ data compared to modeling it with a Coulomb-only curve for use in the residuals treatment (see Sec. **??**).

All of the figures follow the same four-panel structure: [Top Left]: $\Im f_0$ vs. $\Re f_0$, together with d_0 to the right. [Top Right (Bottom Left, Bottom Right)]: λ vs. Radius for the 0-10% (10-30%, 30-50%) bin. The ΛK^{+} system is always presented with red markers, the ΛK^{-} with blue, and the ΛK^{0}_{S} with black. In the case of all ΛK analyses sharing radii, the markers are gold. In the case of only the $\Lambda K^{\pm}$ analyses sharing radii, the markers are magenta. The square symbols in the first column of the legends are to signify the color scheme. The black symbols in the second column of the legend describe the fit procedure used.

To better explain the description in the legends, take Fig. **??** as an example. The square symbols in the first column of the top left figure indicate that the ΛK^{+} scattering parameters are shown in red, the ΛK^{-} in blue, and the ΛK^{0}_{S} in black. The symbols in the second column of the top left figure indicate that the case of three residual contributors is shown with closed circles, ten residual contributors with open crosses, and no residuals with open triangles. For the λ vs. radii plots, the square symbol describing the color scheme in the first column of the top right figure shows that all ΛK analyses share common radii and are shown with gold markers.

Fig. **??** is a bit more involved example, in terms of the markers, so it is worthwhile to explain as a second example. The square symbols in the first column of the top left figure indicate that the ΛK^{+} scattering parameters are shown in red, the ΛK^{-} in blue, and the ΛK^{0}_{S} in black. The symbols in the second column of the top left figure indicate that the case where all ΛK analyses share common radii is shown with closed circles, the case of only $\Lambda K^{\pm}$ analyses sharing radii is shown with open crosses, and the ΛK^{0}_{S} system being fit alone is shown with open triangles. For the λ vs. radii plots, the square symbols describing the color scheme in the first column of the top right figure show that the case where all ΛK analyses share common radii is drawn with gold (in addition to being closed circles, as just described) markers, only $\Lambda K^{\pm}$ analyses sharing radii is shown with magenta (in addition to open crosses, as just described) markers, and the ΛK^{0}_{S} system being fit alone is shown with black (in addition to open triangles, as just described) markers.

Fig. **??** shows a comparison of results obtained using three, ten, and no residual contributors. A more detailed look of the fit with the experimental data can be found in Appendices **??** - **??**. As shown, the scattering parameters vary significantly between the different cases. For the case of no residual contributors, we would expect the $\lambda_{\rm Fit}$ parameters to be closer to $\lambda_{\rm Fit} \sim 0.5$, when considering the value extracted for primary pairs using simulation in Table **??**. For the case of 10 residual contributors, the figure shows the magnitude of the scattering parameters tends to increase, as do the $\lambda_{\rm Fit}$ parameters. The improper treatment of the residuals places less emphasis on the primary interaction, as conveyed through the relative strength of the $\lambda_{\rm Fit}$ parameters between the three and ten residuals case, presented in Tab. **??**. More emphasis is placed on the residual contributors, whose signal is effectively flattened after being run through the appropriate transform matrices (as shown in Figs. **??** and **??** of Sec. **??**). This leads to a lot of mostly flat contributions, as shown e.g. in Fig. **??** in App. **??**. These two effects could account for the (mostly) larger in magnitude scattering parameters and $\lambda_{\rm Fit}$ parameters extracted when assuming 10 residual contributors.

In Fig. **??** we demonstrate the effect of fixing the overall $\lambda_{\rm Fit}$ parameter compared to allowing it to be

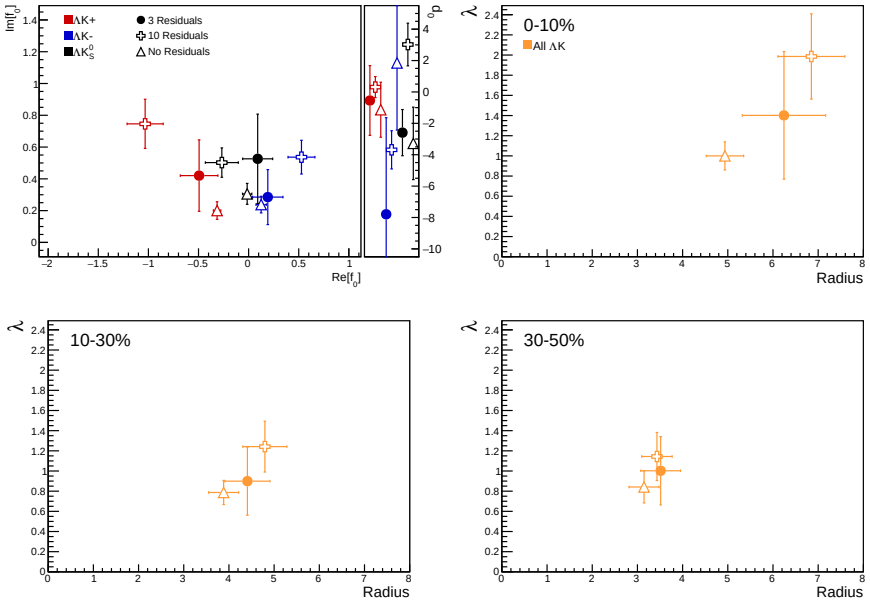

Fig. 18: Results shown for the case of 3 (closer, circles), 10 (open, crosses), and no (open, triangles) residual contributors included in the fit. See text at beginning of section for color scheme information.

free (see Eq. **??** in Sec. **??**). As shown, the extracted scattering parameters are mostly unaffected by this choice. The radii behave as expected, when considering the $\lambda_{\rm Fit}$ and R parameters are strongly correlated. For instance, forcing $\lambda_{\rm Fit}$ to decrease, as in the 0-10% centrality bin shown in the top right of the figure, causes the fit radius to also decrease.

Fig. **??** compares our normal fit results to those obtained when the correlation functions are built using the Stavinskiy method (see Sec. **??**). As shown in the figure, with the exception of the d_0 parameters (which are difficult for us to resolve experimentally), the results from the two methods are within errors of each other. As implemented in this analysis, the Stavinskiy method does a good job of reducing the non-femtoscopic background, but does not completely eliminate it. Nonetheless, it is a simple and elegant method, and should be investigated further in the future.

Fig. **??** shows the different between sharing radii among all ΛK systems versus only sharing radii between the $\Lambda K^{\pm}$ systems. As shown in the figure, the $\Lambda K^{\pm}$ systems give consistent results whether or not the ΛK^0_S system is included in the fit. The ΛK^0_S system, however, gives significantly different results when fit by itself. The ΛK^0_S system suffers the most from low statistics, and is the most difficult to fit (for instance, when fit by itself, the $\lambda_{\rm Fit}$ parameter has to be limited between [0.6, 1.1] to give realistic results). As shown, when fit alone, the ΛK^0_S fit settles on much smaller radii compared to the $\Lambda K^{\pm}$ systems. As we expect the ΛK^0_S system to share similar radii with the $\Lambda K^{\pm}$ systems, we chose to join the three together to combat the low statistics available to the ΛK^0_S. The purpose of this figure is mainly to demonstrate how the inclusion of the ΛK^0_S affects the $\Lambda K^{\pm}$ results, not the other way around.

Finally, Fig. **??** shows the effect of using the experimental $\Xi^-K^{\pm}$ data compared to modeling it with a Coulomb-only curve for use in the residuals treatment (see Sec. **??**). As shown, the results are consistent. The use of a the experimental data is preferable in that no assumption need to be made about the parent system's correlation function. However, the low statistics of the parent $\Xi^-K^{\pm}$ data (especially in the 30-50% centrality bin) could be reason to instead use the Coulomb-only curve. In our description, we choose to use the experimental data, although, as shown in the figure, the choice does not matter much.

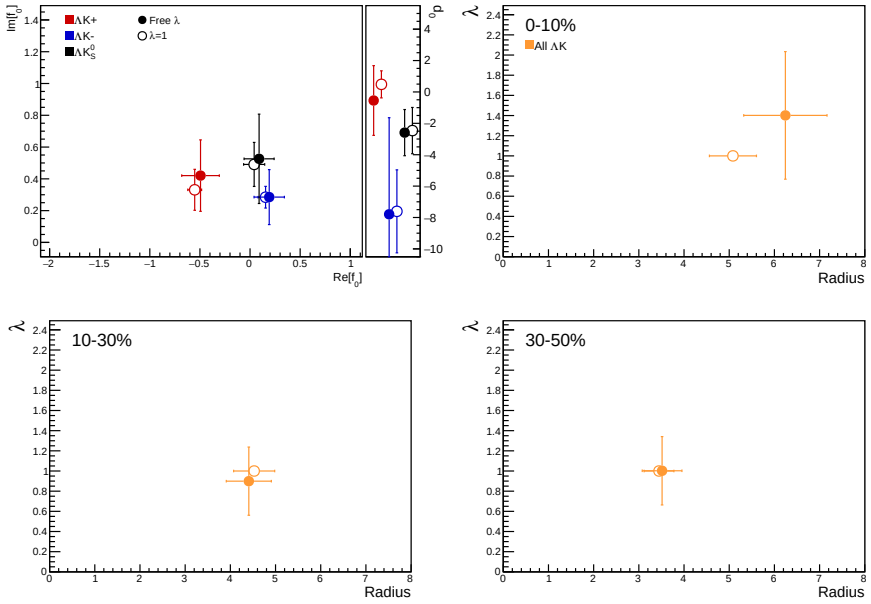

Fig. 19: Results shown for λ_{Fit} parameters left free (closed, circles) and fixed to 1 (open, circles). See text at beginning of section for color scheme information and Eq. **??** in Sec. **??** for more information on the λ_{Fit} parameter.

1.1.5 Discussion of m_{T}-Scaling

It is clear from the results presented in the previous sections, that the ΛK systems do not conform to the approximate m_{T}-scaling of the pair source sizes. At first thought, this may appear to be a troubling result; the approximate scaling is an observed consequence of the collective behavior of the soft (low-p_{T}) sector of the produced system. The Λ and K particles certainly participate in the collective expansion of the QGP medium, so why do their extracted femtoscopic radii not behave as expected? To get straight to the point: the ΛK systems are (obviously) comprised on non-identical particles, each with its own and unique single particle source. Each source is, in general, unique in both its overall size, and in its space-time position within the produced medium. The hydrodynamic nature of the medium produces the approximate m_{T}-scaling with respect to these single-particle sources, not the pair sources. The combination of these effects, when probing correlations between non-identical particle pairs, leads to extracted radii falling outside of the (identical particle femtoscopy) m_{T}-scaling trend. Figure 26 (which contains the same data as Fig.3), shows again the R_{inv} vs m_{T} plot, but also highlights (with arrows) the approximate individual $\langle m_{\text{T}} \rangle$ values of the single particle distributions. The grey circles show how to single particle sizes change with m_{T}.

Taking a close look at Fig. 26, one can see that the previously published data (transparent points) are for identical particle analyses only. For these cases, the pair source, probed through femtoscopy, is comprised of two identical sources laying on top of each other. The extracted femtoscopic radii are related to the single particle source sizes by a factor of $\sqrt{2}$, and of course follow the m_{T}-scaling trend. The other (unpublished) non-identical particle femtoscopic study (pΛ) included in the figure, also shows radii deviating from the m_{T}-scaling band. Drawing a comparison with the $\Lambda\bar{\Lambda}$ study shown in Fig. 3 is a bit more complicated; the $\Lambda\bar{\Lambda}$ system, although containing non-identical particles, does contain a particle with its antiparticle, for which annihilation could conceivably alter the pair source distribution. It would be more surprising if the non-identical analyses did happen to conform to the scaling; although, this could occur for a non-identical analysis in which the particles have similar masses as well as similar m_{T} distributions. For the case presented here, the result differing from m_{T}-scaling is not surprising.

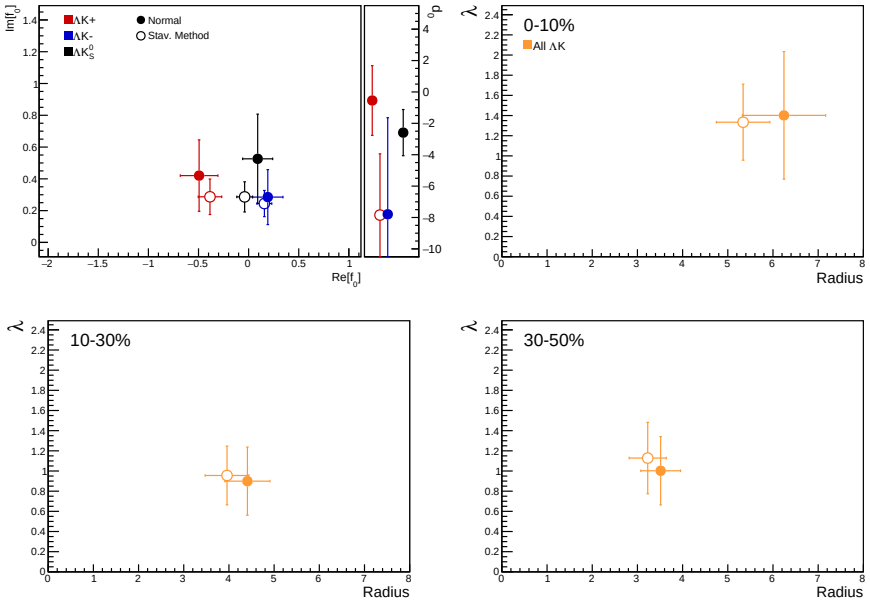

Fig. 20: Results shown for normal correlation function construction (closed, circles) and when built using the Stavinskiy method (open, circles). See text at beginning of section for color scheme information and Sec. **??** for more information on the Stavinskiy method.

I will also briefly point out that it is not automatically clear where a non-identical study should be placed on such a R_{inv} vs m_{T} plot. Each single particle distribution has a well-defined $\langle m_{\text{T}} \rangle$, which, to a large extent, determines the single particle region of homogeneity. When combining two sources with different spatio-temporal characteristics, originating from particles of different m_{T}, how should one define the pair m_{T}? A simple mathematical expression for the pair m_{T} is easy to come up with, but that's not exactly what I'm hinting at here. With respect to this m_{T}-scaling picture, the m_{T} value dictates the source size, and one desires the same for non-identical particles. However, do the two unequal sized sources both contribute equally to the extracted femtoscopic size? Or does the larger (smaller) source more closely dictate the femtoscopic signal? If the contribution is equal, then it seems natural to simply more-or-less average the two, single particle, m_{T} values. If the contribution is unequal, then there should be introduced some sore of weighting in the pair m_{T} calculation reflecting this fact. In any case, in our study we use the most straightforward definition of pair m_{T}, defined as:

$$m^2_{\text{T,pair}} = \left(\frac{m_{\text{inv}}}{2}\right)^2 + \left(\frac{1}{2}|\boldsymbol{p}_{\text{T},1} + \boldsymbol{p}_{\text{T},2}|\right)^2 \tag{1}$$

Many times, the equation for non-identical particle pair m_{T} is defined with the average mass replacing $m_{\text{inv}}/2$. However, the above Eq. 1 is more directly analogous to the single particle m_{T}:

$$m^2_{\text{T}} = m^2 + \boldsymbol{p}^2_{\text{T}} = (p^0)^2 - (p^3)^2 \tag{2}$$

as, Eq. 1 may be rewritten as:

$$\begin{aligned} m^2_{\text{T,pair}} &= (K^0)^2 - (K^3)^2 \\ K^\mu &\equiv \frac{1}{2}\left(p^\mu_1 + p^\mu_2\right) \end{aligned} \tag{3}$$

Identical particle femtoscopic studies are able to probe only the size of the emitting region, or, more

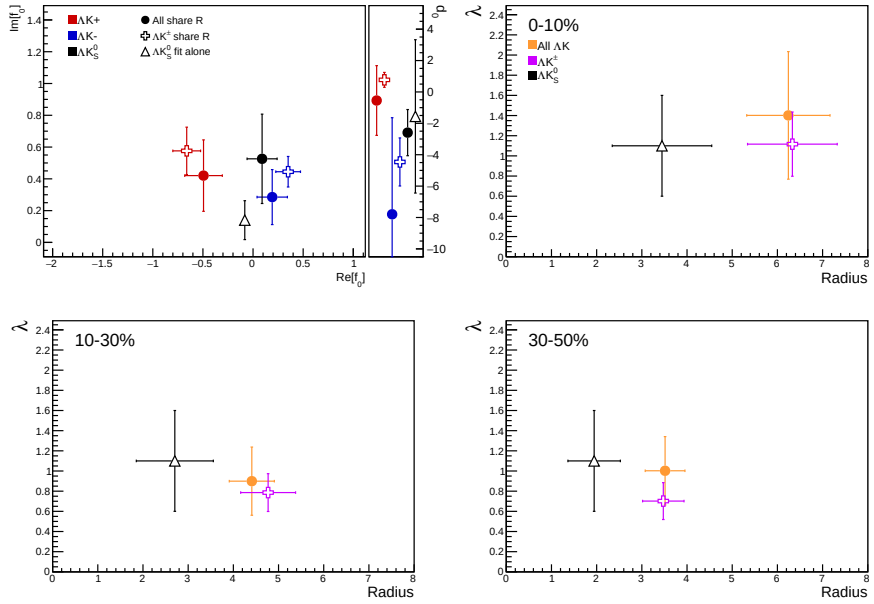

Fig. 21: Results shown for the case of all ΛK analyses sharing radii (closed, circles) and only the $\Lambda K^{\pm}$ analyses sharing radii (open, crossed), with the ΛK^0_S system fit separately (open, triangles). See text at beginning of section for color scheme information.

precisely, the second moments of the emission function. In addition to this, non-identical particle studies are able to measure the relative emission shifts, the first moments of the emission function. One method to extract information about the emission asymmetries in the system is via a spherical decomposition of the correlation function. With this method, one can draw a wealth of information from just a few components of the decomposition. More specifically, the C_{00} component is similar to the 1D correlation functions typically studied, and probes the overall size of the source. The $\Re C_{11}$ component probes the asymmetry in the system; a non-zero value reveals the asymmetry.

In Fig. 27 we show results for the C_{00} and $\Re C_{11}$ components from the spherical decomposition of our ΛK^+ system in the 0-10% centrality bin (red circles). Results from a number of other components within the decomposition, as well as for our ΛK^0_S and ΛK^- systems, are contained in **??**. Along with the experimental data in Fig. 27, we have also included results from THERMINATOR simulation for an impact parameter of b = 2 fm (gold stars). As THERMINATOR does not include any final state effects, we assumed scattering parameters ($\Re f_0, \Im f_0, d_0$) = (-1.16, 0.51, 1.08) and weighted the numerator pairs with $|\Psi|^2$, as discussed previously. As seen in the figure, the C_{00} signal is similar to that observed in our one-dimensional study. The $\Re C_{11}$ component shows a clear deviation from zero, and the negative value signifies that the Λ particles are, on average, emitted further out and/or earlier than the K mesons.

Fig. 28 shows a closer look at the THERMINATOR simulation, whose spherical harmonic decomposition was shown along with the data in Fig. 27. The top left of Fig. 28a shows a fit to the one-dimensional correlation function from THERMINATOR. The scattering parameters are known precisely here, as they served as the weights used in the simulation, and are kept constant in the fit. We are interested in looking at the extracted one-dimensional source size here, so the λ parameter is also fixed at unity. The other three plots in Fig. 28a show the source distribution in the out (top right), side (bottom left), and long (bottom right) directions (all in the PRF). The source distributions have all been fitted with a Gaussian form, the result of which is printed within the respective plot. One immediately sees a significant shift in the out direction, $\mu_{\text{out}} \approx 4$ fm, and negligible shift in the other two directions, $\mu_{\text{side}} \approx \mu_{\text{long}} \approx 0$ fm. The figure demonstrates that, within the THERMINATOR model, the Λ is, on average, emitted further out that its K partner. Finally, Fig. 28b shows the distribution of the relative time of emittance, again in

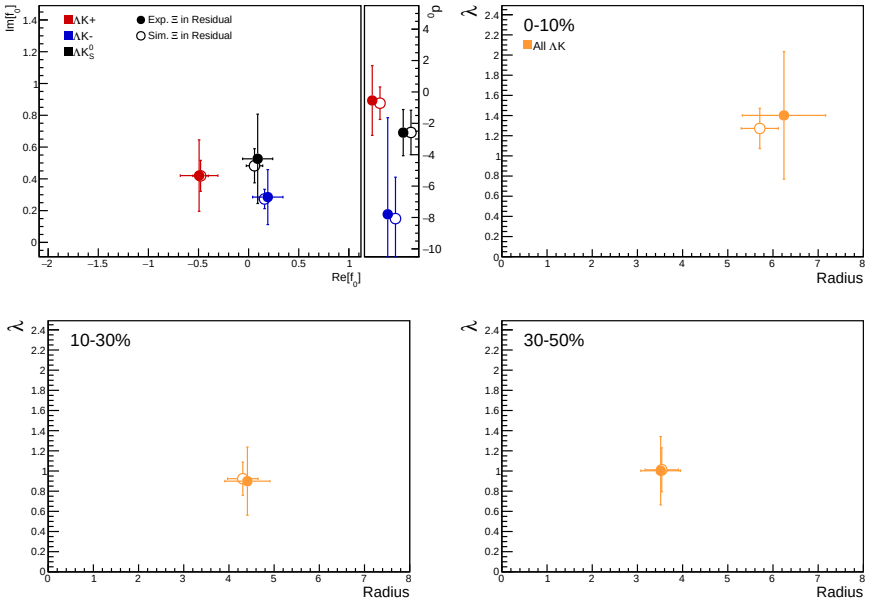

Fig. 22: Results shown when using experimental $\Xi^-K^\pm$ data (closed, circles) and when simulating the $\Xi^-K^\pm$ correlation function with a Coulomb-only curve (open, circles) for use in the treatment of the residual. See text at beginning of section for color scheme information, and Sec. **??** for more information on the $\Xi^-K^\pm$ simulation.

the PRF. The figure shows that the Λ is, on average, emitted earlier than its K partner.

We end this section with a brief look at how a spatial separation of the single particle sources affects the radii extracted from a femtoscopic analysis. To achieve this, we use THERMINATOR in a similar fashion as described above, but with one important difference. Instead of taking the source information from THERMINATOR, we instead draw the source from a pre-determined Gaussian distribution. In all cases, we take $R_{\rm out} = R_{\rm side} = R_{\rm long}$ = 5 fm, and $\mu_{\rm side} = \mu_{\rm long}$ = 0 fm. Figure 29 shows an example of results obtained from THERMINATOR following this procedure, where $\mu_{\rm out}$ = 3 fm.

In Figure 30, we show results for the case of μ_{out} = 1 fm, μ_{out} = 3 fm, and μ_{out} = 6 fm. In this figure, we do not show the side and long distributions, as they appear identical to those shown in Fig. 29. The figure demonstrates that as the separation μ_{out} increases, so do the extracted femtoscopic radii.

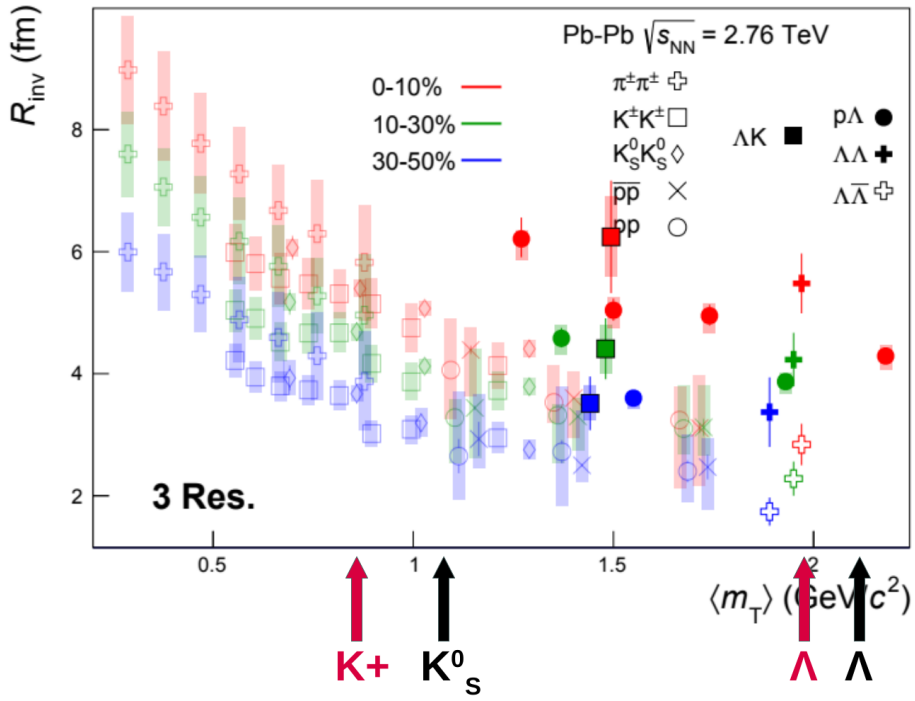

Fig. 23: Same as Fig. 3, but with the individual m_T values for the single particle distributions identified. The grey circles show how the single particle sizes are expected to change with m_T.

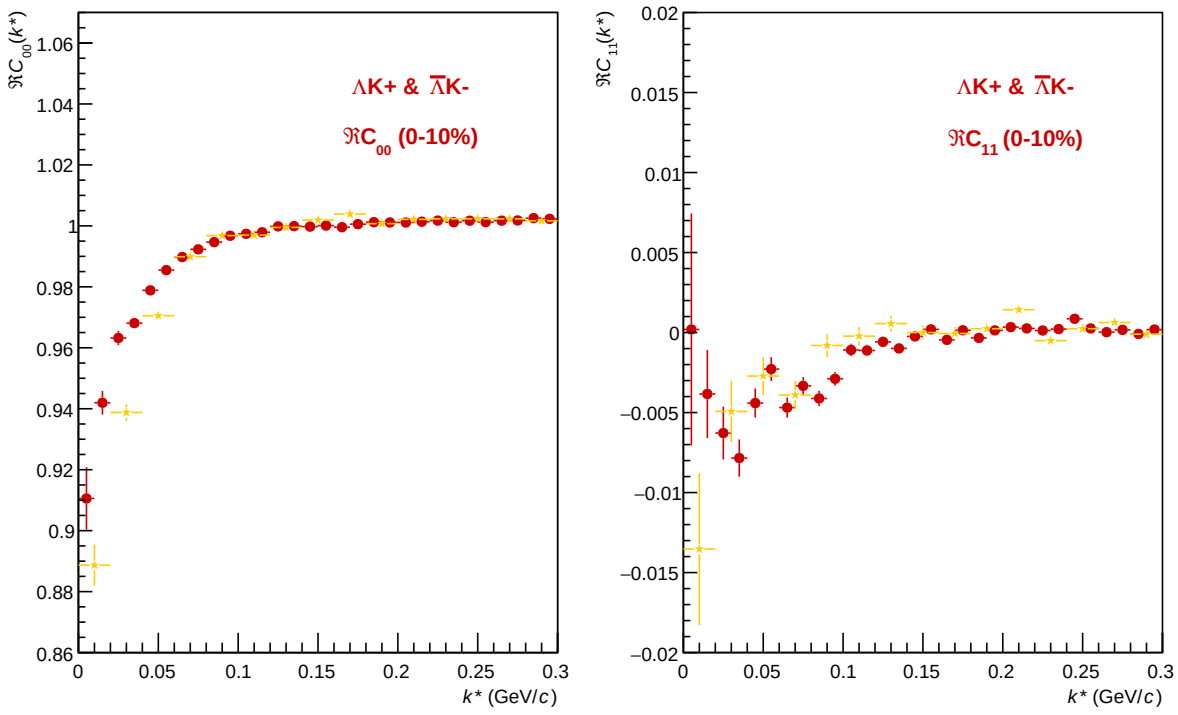

Fig. 24: C_{00} (left) and $\Re C_{11}$ (right) components of a spherical harmonic decomposition of the ΛK^+ correlation function for the 0-10% centrality bin. The C_{00} component is similar to the 1D correlation functions typically studied, and probes the overall size of the source. The $\Re C_{11}$ component probes the asymmetry in the system; a non-zero value reveals the asymmetry

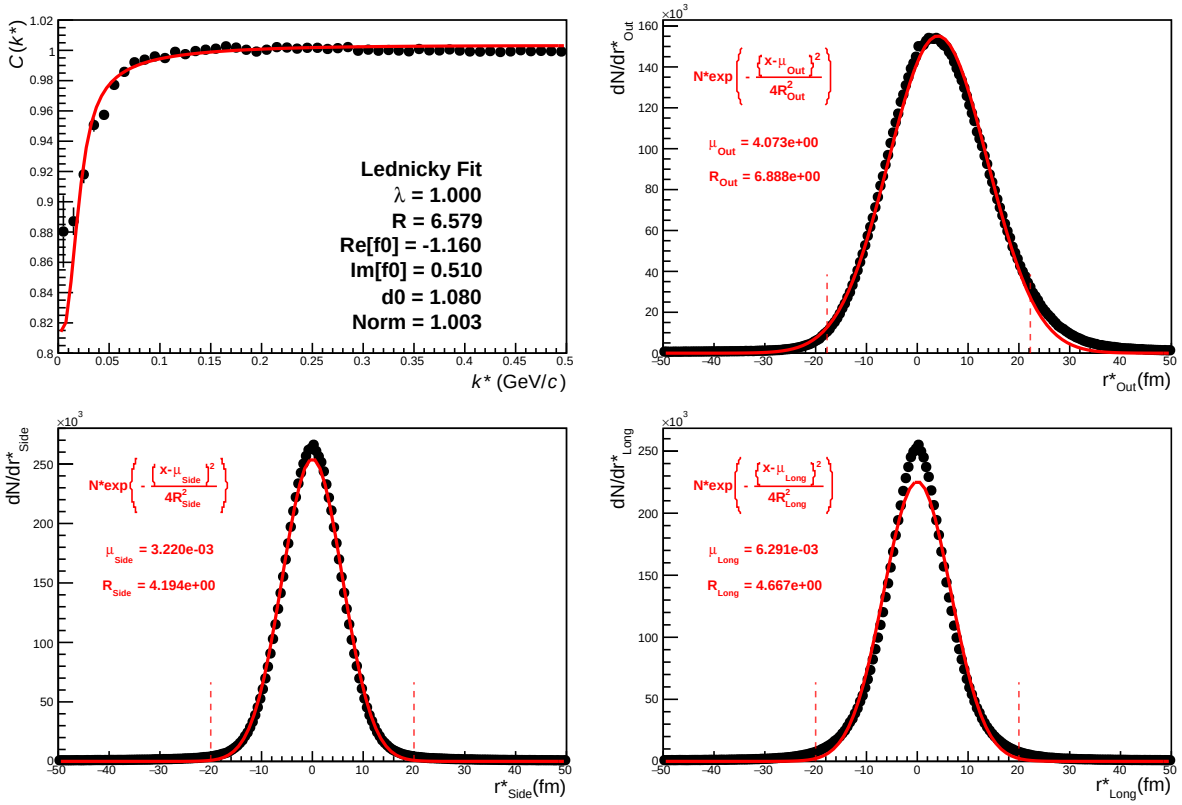

(a) Caption 1

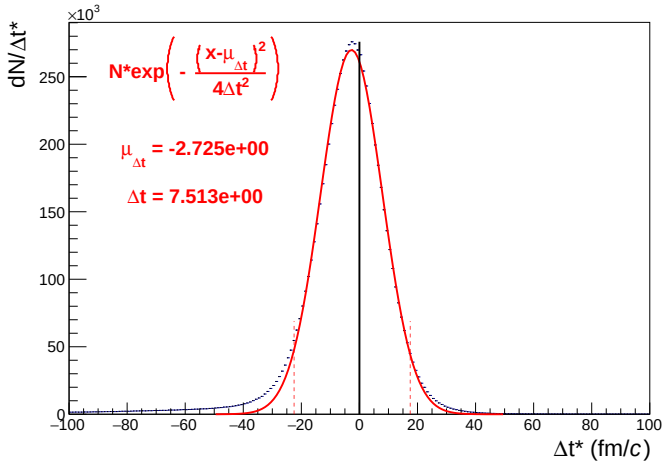

(b) Caption 2

Fig. 25: Long Overall

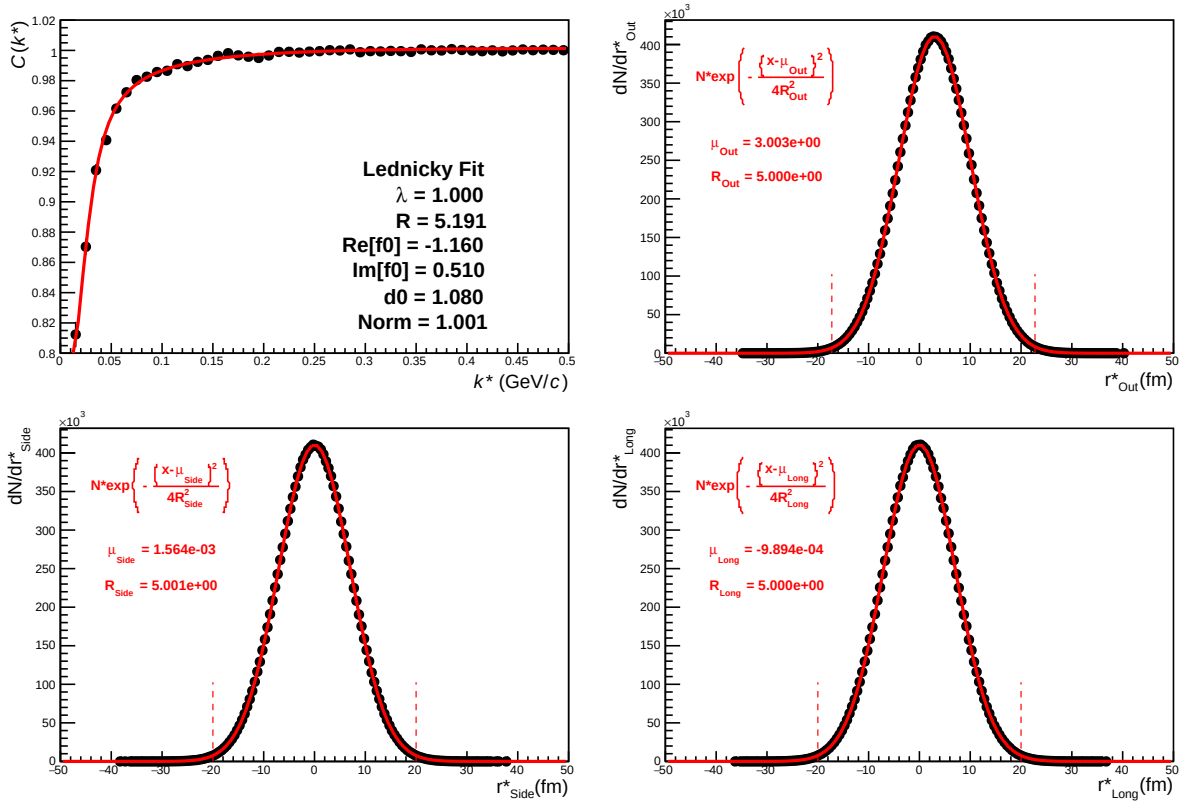

Fig. 26: Long Caption

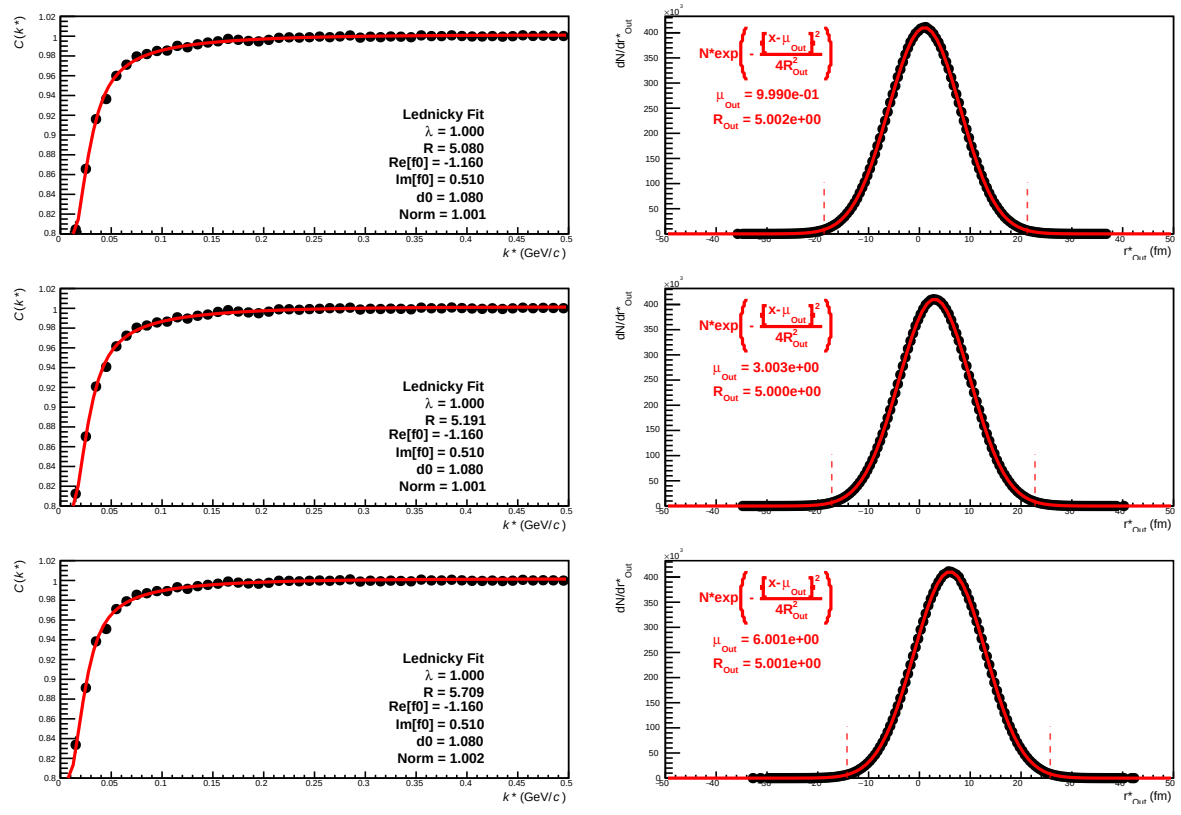

Fig. 27: Long Caption

1.2 Results: $\Xi K^{\pm}$

Even without any fits to the data, the fact that the $\Xi^{-}K^{+}$ data dips below unity (Fig. 31) is exciting, as this cannot occur purely from a Coulomb interaction. We hope that this dip signifies that we are able to peer through the overwhelming contribution from the Coulomb interaction to see the effects arising from the strong interaction.

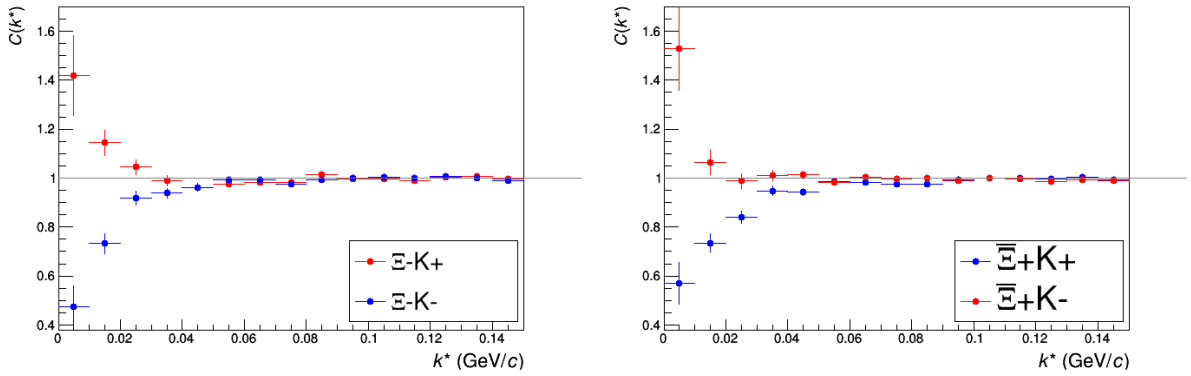

Fig. 28: $\Xi K^{\pm}$ Results for 0-10% Centrality. (Left) $\Xi^{-}K^{+}$ and $\Xi^{-}K^{-}$ (Right) $\bar{\Xi}^{+}K^{+}$ and $\bar{\Xi}^{+}K^{-}$

Figure 32 demonstrates graphically, that the $\Xi^{-}K^{+}$ results cannot be described by solely the Coulomb interaction. In this figure, we present the data along with a Coulomb-only band. The Coulomb-only band is spanned by two Coulomb-only curves, whose parameters are given in the figure. The Coulomb-only curves were generated using a technique identical to the generation of the fit function, described in Sec. **??**, except, of course, with the nuclear scattering parameters all set to zero. The Coulomb-only curves change monotonically with varying λ or varyin radius parametres, therefore, any curves built with parameter sets intermediate to those use in the Coulomb-only band will be contained in the band.

Including the strong interaction into the simulation can change, sometimes dramatically, the resulting correlation function, as shown in Figure 33. In the figure, the solid line represents a Coulomb-only curve, i.e. a simulated correlation function with the strong interaction turned off. The dashed lines represent a full simulation, including both the strong and Coulomb interactions. The two dashed lines differ only in the real part of the assumed scattering length: positive in Set 1, and negative in Set 2. In the top figure, for the $\Xi^{-}K^{+}$ simulation, we see that parameter set 2, with a negative real part of the scattering length, causes the simulated curve to dip below unity, as is seen in the data. If there is a parallel to be drawn between this analysis and the ΛK analysis, we expect to see similar effects in the $\Lambda K+$ system and the $\Xi^{-}K^{+}$ systems. In these systems, we could have an $s\bar{s}$ annihilation picture. Or, another possible way of thinking about these systems is in terms of net strangeness. The ΛK^{+} system has S=0, while the ΛK^{-} has S=-2. The $\Xi^{-}K^{+}$ has S=-1, while the $\Xi^{-}K^{-}$ has S=-3.

The author was asked to perform a global Coulomb-only fit to the data, to ensure that the system truly could not be described simply by the Coulomb interaction. In order words, in the fit, the strong force was turned off, and the $\Xi^{-}K^{+}$, $\bar{\Xi}^{+}K^{-}$, $\Xi^{-}K^{-}$, $\bar{\Xi}^{+}K^{+}$ systems all share one sinlge radius parameter, while the pair and conjugate pair systems share a λ parameter. The results of this fit are shown in Figures 34 and 35. In Fig. 34, there was a lower limit of 0.1 fm placed on the radius parameter, and the radius parameter was initialized to 3 fm (as seems reasonable, when considering the transverse mass of the system and looking at Fig. 3). As is shown in the results, the radius parameter reached this unrealistic lower bound of 0.1 fm. In Fig. 35, the parameters were all unbounded, and the radius parameter was initialized to 10 fm. In this case, the radius parameters reamins high, and ends at an unrealistic value of 10.84 fm. In both cases, the λ parameters are too low. From these figures, we conclude that a global Coulomb-only fit is not suitable for the data.

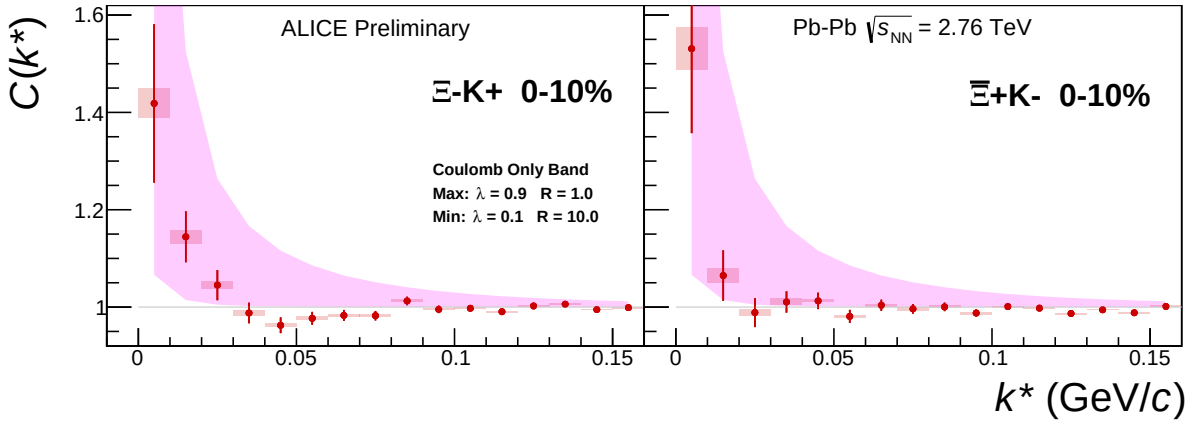

(a) (Left) ΞK^+ and (Right) $\bar{\Xi}K^-$

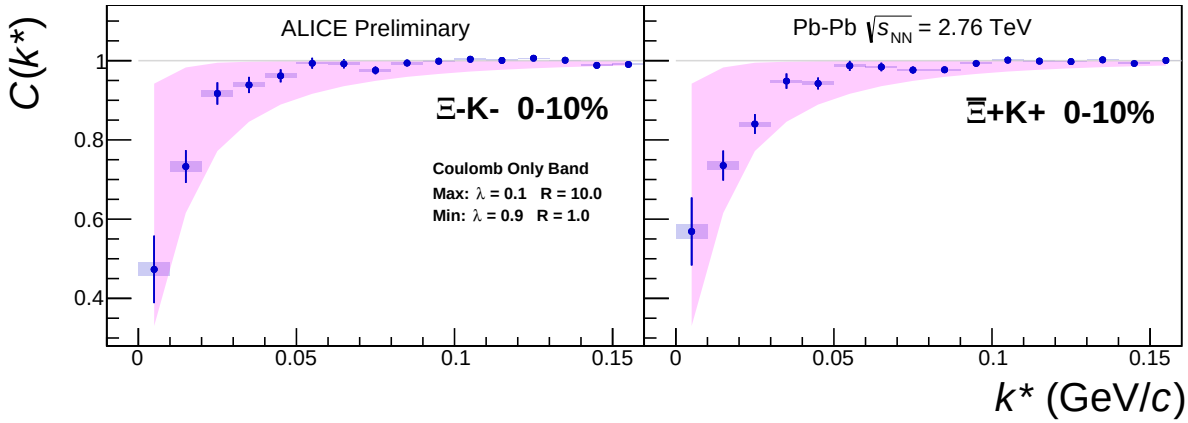

(b) (Left) ΞK^- and (Right) $\bar{\Xi}K^+$

Fig. 29: $\Xi K^{\pm}$ data with Coulomb-only bands for the 0-10% centrality bin. The Coulomb-only bands span two sets of Coulomb-only curves: (1) λ = 0.9, R = 1.0 fm and (2) λ = 0.1, R = 10.0 fm. The Coulomb-only curves are simulated correlation functions for the respective pair system assuming only a Coulomb interaction, i.e. ignoring the strong interaction. The Coulomb-only curves change monotonically with varying λ and varying R, therefore, any intermediate parameter set will fall within this Coulomb-only band.

Although the global Coulomb-only fit failed, it is possible that a Coulomb-only fit performed on Ξ^-K^+ and $\bar{\Xi}^+K^-$ separately from Ξ^-K^- and $\bar{\Xi}^+K^+$ could be suitable. The result of such fits are shown in Figures 36 and 37. Figure 36, shows that the fit is not able to describe the dip in the Ξ^-K^+ data below unity. Of course, this is obviously true for an attractive Coulomb-only fit. The radius parameter of 8.43 fm extracted from this fit is unrealistically large. In Figure 37 shows the Coulomb-only fit can described the Ξ^-K^- data reasonable well; although the extracted radius of 3.73 fm is somewhat larger than expected.

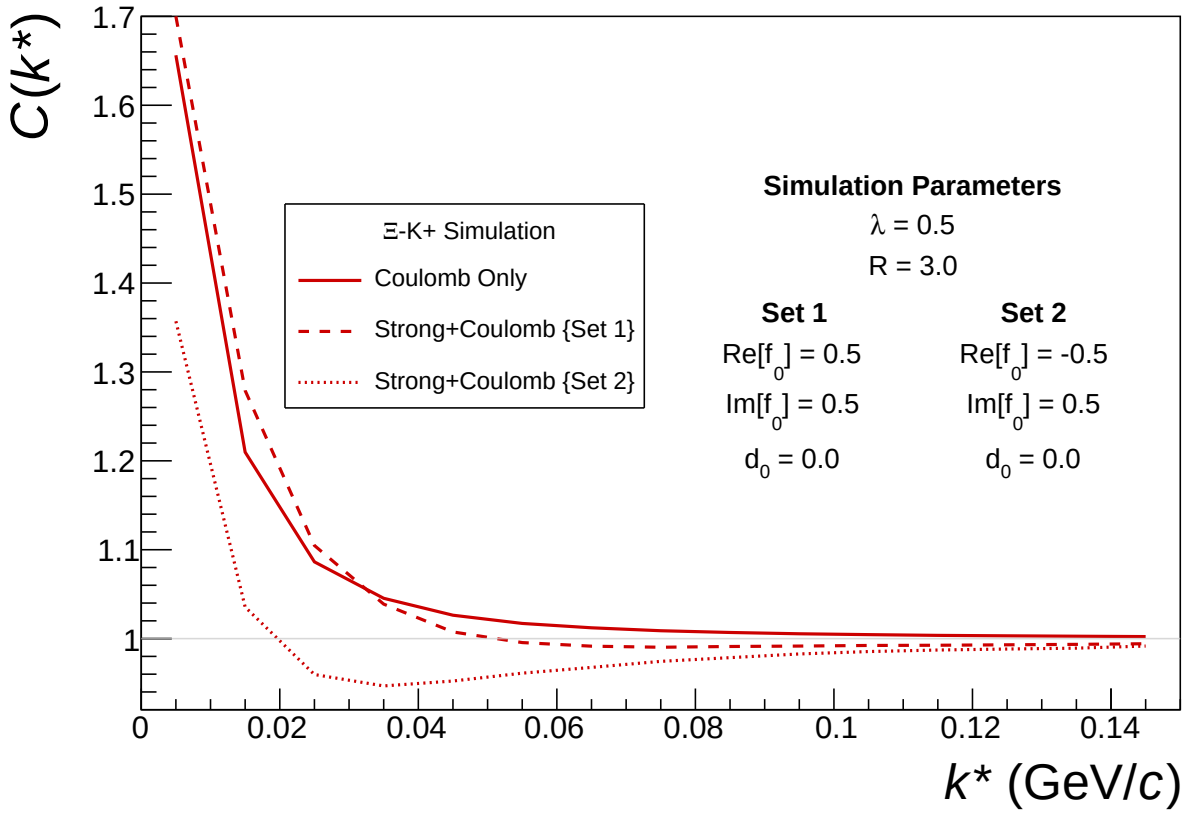

(a) ΞK^+ and $\bar{\Xi} K^-$ simulation

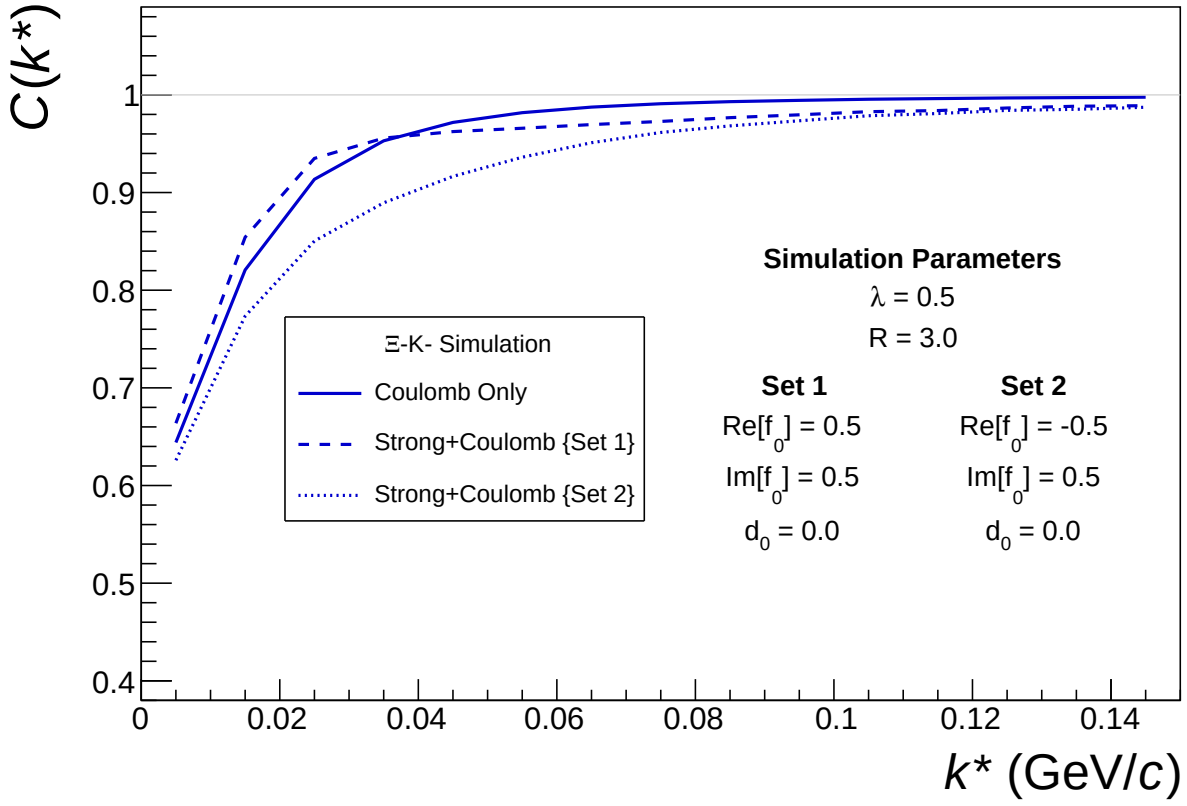

(b) ΞK^- and $\bar{\Xi} K^+$ simulation

Fig. 30: Effect on the Coulomb-only curve of including the strong interaction for $\Xi K^{\pm}$ systems. The solid line represents a Coulomb-only curve, i.e. a simulated correlation function with the strong interaction turned off. The dashed lines represent a full simulation, including both the strong and Coulomb interactions. The two dashed lines differ only in the real part of the assumed scattering length: positive in Set 1, and negative in Set 2.

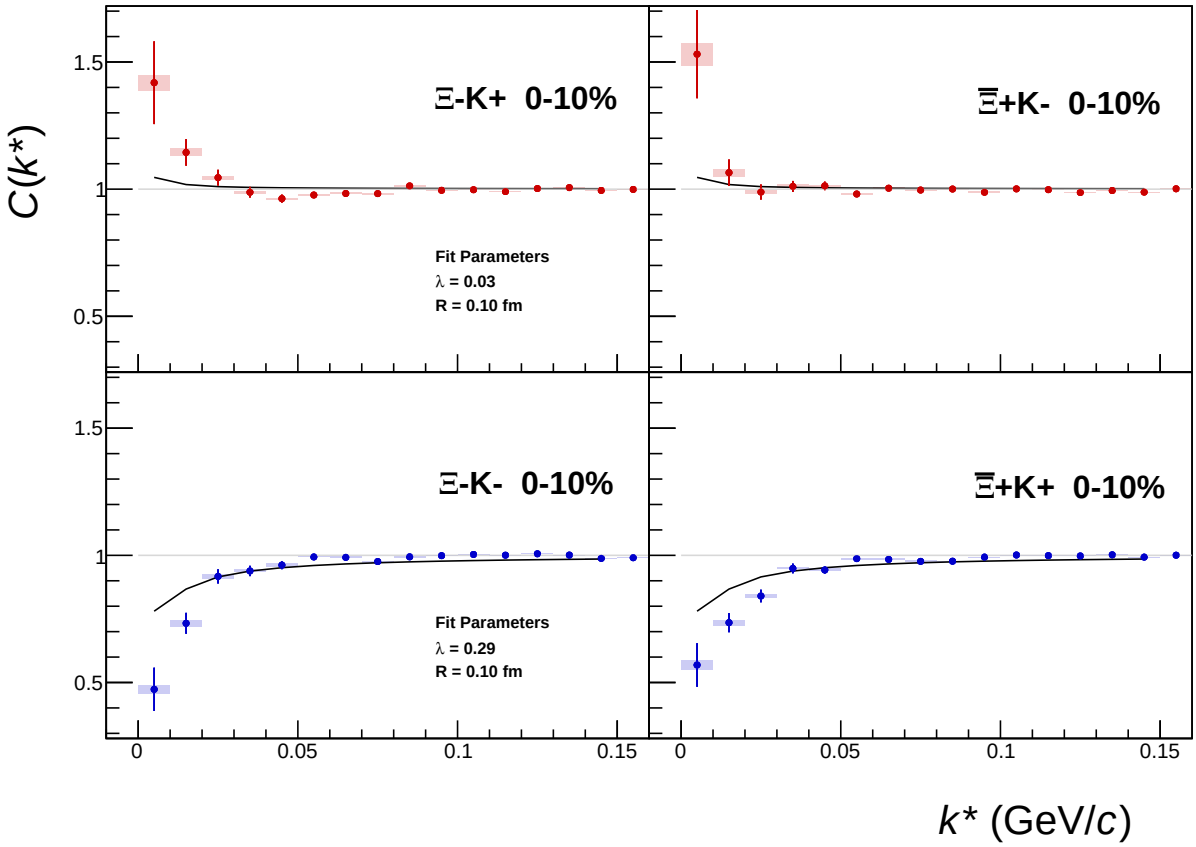

Fig. 31: $\Xi K^{\pm}$ Global Coulomb-only fit (Set 1) for 0-10% centrality. In this fit, there was a lower limit of 0.1 fm placed on the radius parameter, and the radius parameter was initialized to 3 fm (as seems reasonable, when considering the transverse mass of the system and looking at Fig. 3). As is shown in the results, the radius parameter reached this unrealistic lower bound of 0.1 fm. Also, the extracted λ parameters are too low.

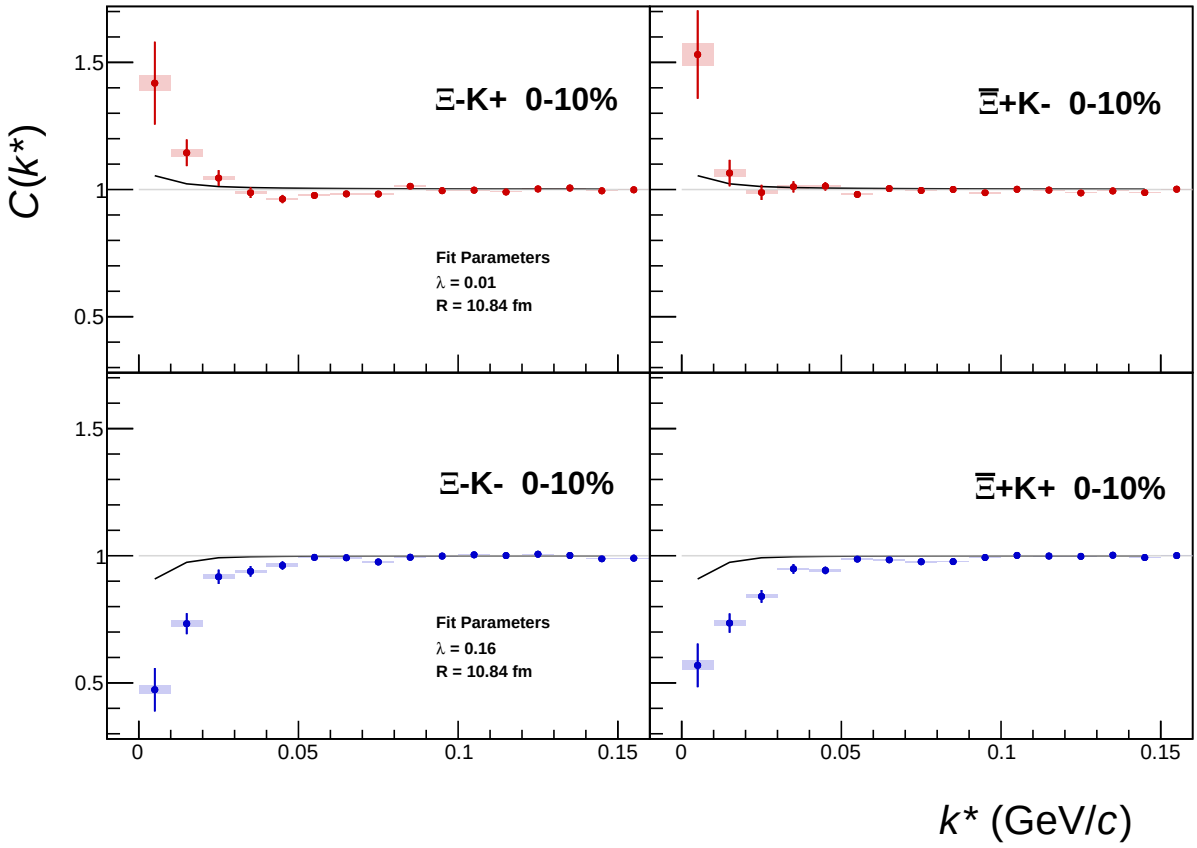

Fig. 32: $\Xi K^{\pm}$ Global Coulomb-only fit (Set 2) for 0-10% centrality. In this fit, the parameters were all unbounded, and the radius parameter was initialized to 10 fm. In this case, the radius parameters reamins high, and ends at an unrealistic value of 10.84 fm. Also, the extracted λ parameters are too low.

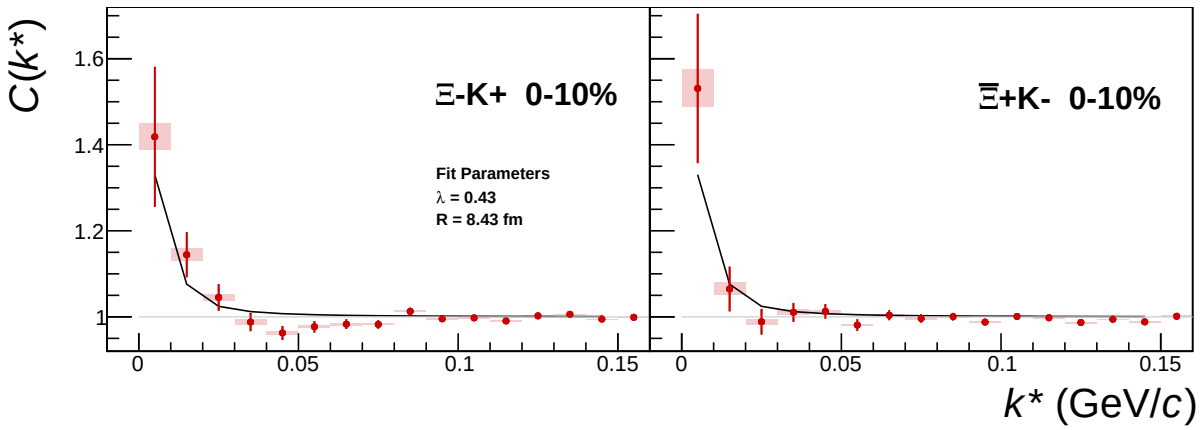

Fig. 33: $\Xi^{-}K^{+}$ Coulomb-only fit for 0-10% centrality

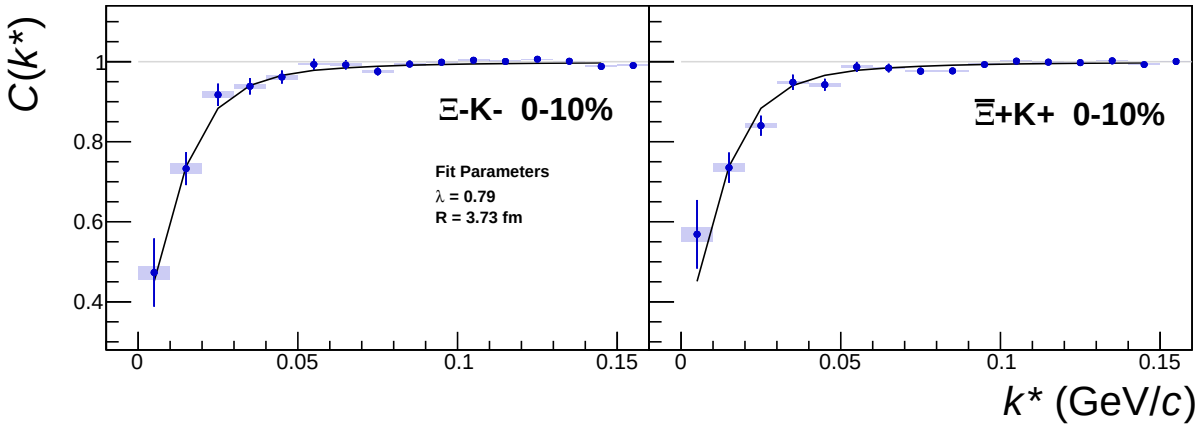

Fig. 34: $\Xi^-\mathrm{K}^-$ Coulomb-only fit for 0-10% centrality